ADVANCED HEALTHCARE MATERIALS
www.advhealthmat.de

Natural Polymer-Polyphenol Bioadhesive Coacervate with Stable Wet Adhesion, Antibacterial Activity, and On-Demand Detachment

Margarida M. A. Sacramento, Mariana B. Oliveira, José R.B. Gomes, João Borges, Benjamin R. Freedman, David J. Mooney, João M. M. Rodrigues, and João F. Mano**

Medical adhesives are emerging as an important clinical tool as adjuvants for sutures and staples in wound closure and healing and in the achievement of hemostasis. However, clinical adhesives combining cytocompatibility, as well as strong and stable adhesion in physiological conditions, are still in demand. Herein, a mussel-inspired strategy is explored to produce adhesive coacervates using tannic acid (TA) and methacrylate pullulan (PUL-MA). TA|PUL-MA coacervates mainly comprise van der Waals forces and hydrophobic interactions. The methacrylic groups in the PUL backbone increase the number of interactions in the adhesives matrix, resulting in enhanced cohesion and adhesion strength (72.7 Jm^{-2}), compared to the non-methacrylated coacervate. The adhesive properties are kept in physiologic-mimetic solutions (72.8 Jm^{-2}) for 72 h. The photopolymerization of TA|PUL-MA enables the on-demand detachment of the adhesive. The poor cytocompatibility associated with the use of phenolic groups is here circumvented by mixing reactive oxygen species-degrading enzyme in the adhesive coacervate. This addition does not hamper the adhesive character of the materials, nor their anti-microbial or hemostatic properties. This affordable and straightforward methodology, together with the tailorable adhesivity even in wet environments, high cytocompatibility, and anti-bacterial activity, enables foresee TA|PUL-MA as a promising ready-to-use bioadhesive for biomedical applications.

1. Introduction

Tissue adhesives have emerged as important tools for medical applications, serving as surgical sealants,[1] hemostatic agents,[2] adjuvants in the first stage of wound healing,[3] or for skin device attachment applications.[4] They offer remarkable advantages such as ease of operation and reduced surgery times.[5,6] Fibrin sealants, commercially available since 1940, have been extensively used in several surgical procedures, showing high biocompatibility and biodegradability.[7] However, their utility is limited as they are prone to rupture and debonding. In contrast, cyanoacrylates-based adhesives enable strong tissue adhesion, although their cytotoxicity, poor deformability, and high stiffness are well-reported factors that limit their application.[8]

The mussel's adhesion mechanism based on the amino acid 3,4-dihydroxy-L-phenylalanine (L-DOPA), has been an extraordinary source of inspiration for the development of an extensive library of advanced adhesive biomaterials by

M. M. A. Sacramento, M. B. Oliveira, J. R. Gomes, J. Borges, J. M. M. Rodrigues, J. F. Mano
CICECO – Aveiro Institute of Materials
Department of Chemistry
University of Aveiro
Campus Universitário de Santiago
Aveiro 3810-193, Portugal
E-mail: jrodrigues@ua.pt; jmano@ua.pt

B. R. Freedman, D. J. Mooney
John A. Paulson School of Engineering and Applied Sciences
Harvard University
Cambridge, MA 02138, USA

B. R. Freedman, D. J. Mooney
Wyss Institute for Biologically Inspired Engineering
Harvard University
Cambridge, MA 02138, USA

B. R. Freedman
Department of Orthopaedic Surgery
Beth Israel Deaconess Medical Center
Harvard Medical School
Boston, MA 02215, USA

The ORCID identification number(s) for the author(s) of this article can be found under https://doi.org/10.1002/adhm.202304587

DOI: 10.1002/adhm.202304587

exploring the catechol-based chemistries.[9,10] Nonetheless, cell toxicity, along with antimicrobial activity, has been occasionally reported for these materials. The free integration of catechol groups culminates in their autooxidation in physiological pH conditions, leading to the production of reactive oxygen species (ROS), hypothesized to induce cytotoxicity.[11,12] Strategies to mitigate the cytotoxic effect of catechol-modified materials have comprised either the hampering of oxidation through metal ion coordination or the addition of exogenous molecules or materials to limit the action of the formed reactive species (e.g., the addition of ROS-degrading enzymes).[13–16] Interestingly, although some of these strategies have proven effective in improving the cytocompatibility of catechol-based adhesives, the maintenance of adhesion potential and antimicrobial effect of these constructs after such treatments has not been fully explored.

Here, the exploration of a completely natural adhesive prepared from off-the-shelf materials is addressed concerning the processing requirements needed for the achievement of concomitant adequate tissue adhesion, cytocompatibility, maintenance of antimicrobial effect, and hemostatic behavior. The proposed methodology is based on the spontaneous coacervation of a polyphenol with a natural polysaccharide. In fact, resorting to the biomimetic mussel-inspired formation of coacervates for the fabrication of bioadhesives has been associated with higher tissue adhesion due to the increased cohesion of the material.[5,17,18] For the proof of concept, we explore a straightforward and affordable system composed uniquely of natural compounds: tannic acid (TA) and a high-molecular-weight natural polymer – pullulan (PUL). The latter is a non-ionic linear polysaccharide with inherent slightly adhesive properties,[19] and both components have the Generally Regarded as Safe (GRAS) classification by the FDA.[5,20] The functionalization of PUL with pendant methacrylic groups, applied without photopolymerization, enabled increased cohesion and adhesion strength of about threefold when compared to a fibrin sealant.[21,22] TA|PUL-MA adhesive holds a compromise between all the required features for a tissue adhesive, demonstrating a very stable adhesion capacity, even in wet surfaces and immersed tissues, while also ensuring cytocompatibility, anti-microbial properties, and hemostatic behavior. Finally, for the first time, a dual functional property of the methacrylic group is explored and reported, allowing the improvement of the adhesive properties and the easy on-demand detachment upon UV-crosslinking of the adhesive.

2. Results

2.1. Assessment of Coacervate Formation between TA and Natural-Derived Polysaccharides

Coacervation is a phenomenon that consists of the separation of two immiscible liquid phases, that result from the interaction of oppositely charged molecules (i.e., complex coacervates) or from the association of hydrophobic domains.[23] Together with L-DOPA-containing proteins, marine organisms produce extracellular coacervates as a strategy to achieve strong adhesion to underwater surfaces.[24]

We hypothesized that an adhesive could be formulated from the coacervation of a catechol-containing molecule such as TA and polysaccharides. Different nature-derived polysaccharides were combined with the polyphenol at a fixed concentration (i.e., between 5% and 10% w/w depending on their solubility – Table S1, Supporting Information) to investigate the formation of separating phases (Figure S1, Supporting Information). Some combinations presented a turbid appearance immediately after the mixture of the two solutions, suggesting an instant increase in the number of non-covalent interactions established between TA and the polysaccharides (Figure S1, Supporting Information).[25] However, only the combination of PUL with TA originated detectable separating phases, with the sedimentation of a denser phase after 24 h. When compared to the other tested polysaccharides, PUL shows high water-solubility and relatively low viscosity,[26] which combined with its inherent adhesive character,[19] are attractive features that make this polysaccharide an interesting building block for the development of an adhesive system in combination with TA.

To better understand the coacervate TA|PUL system, several formulations were prepared by mixing PUL and TA aqueous solutions at different concentrations (Figure S2, Supporting Information). TA|PUL 20|20 (i.e., 20% (w/w) TA aqueous solution|20% (w/w) PUL aqueous solution) adhesive showed a higher relative volume of coacervate phase formation and, therefore, its dense phase was chosen to proceed with the work.

Multiple noncovalent interactions, that is, H-bonds, metal(oxide) coordination bonds, cation–π interactions, and π–π interactions are involved in the mechanism of mussel adhesion to various surfaces.[27,28] However, these protein-rich adhesive coacervates also comprise hydrophobic domains that are known to play an important role in adhesion.[29] In addition, hydrophobic moieties have been associated with increased interfacial strength between tissues and adhesives.[30–32] Aiming to improve the cohesion and adhesion of the TA|PUL 20|20 adhesive, we hypothesized that the introduction of a partially hydrophobic moiety would improve the properties of the adhesive. Consequently, to maintain the adhesive natural character as much as possible, the polysaccharide fraction was replaced by a slightly chemically modified version, its methacrylated form – PUL-MA (Figure S3ii, Supporting Information). The grafting of methacrylate groups into the polymeric chain is expected to enable light-triggered crosslinking. The effect of an additional photocrosslinking step was hypothesized to increase the coacervates' cohesion, and its effect on the overall adhesive properties of the material was studied. ^{1}H-NMR (Figure S4, Supporting Information) and attenuated total reflectance-Fourier transform infrared (ATR-FTIR) spectroscopy (Figure S5, Supporting Information) confirmed the substitution of the PUL polymeric chains with methacrylate groups at degrees of 6% or 13%. Both conditions were selected for further studies of tissue adhesion, hemostatic properties, antibacterial activity, and cytocompatibility.

2.2. MD Simulations of the Formation of TA|PUL and TA|PUL-MA Coacervate Adhesive System and Rheological Analysis

To shed light on the interaction mechanisms that drove the formation and cohesion of the adhesives, and the influence of the

Table 1. Contribution of each energy term for the establishment of TA|PUL.

Energy term	TA|PUL	TA|PUL-MA	TA|TA	PUL|PUL	PUL-MA|PUL-MA
H-bond	0.71(3.45)	1.18(4.14)	2.34	1.16	1.02
van der Waals	−196.5(−400.1)	−229.9(−552.2)	−252.5	−136.3	−121.5
Electrostatic	−2.3(−5.0)	−1.4 (−11.6)	−3.3	−3.4	−3.6
Polar solvation	29.5 (69.8)	39.1 (98.0)	49.1	22.6	23.7
Non-polar solvation	−19.5(−42.8)	−22.7 (−54.7)	−26.9	−15.1	−15.6
Total binding	−188.7(−378.1)	−214.9(−520.5)	−233.6	−132.2	−117

[a] Average number of H-bonds between the solute molecules per simulation timeframe, using the default cut-off values for donor–acceptor distance (0.35 nm) and hydrogen–donor–acceptor angle (30°); [b] Results in parenthesis are for the 2:3:4000 TA:PUL:water or TA:PUL-MA:water systems; [c] A conservative value of 20 was used for the dielectric constant of the solute molecules in the MM-PBSA calculations. With a tenfold decrease of this value (i.e., 2), the electrostatic energy increases tenfold approximately; [d] Calculated with the solvent accessible surface area (SASA) nonpolar method.

introduction of the methacrylic group on the polymer backbone, molecular dynamics (MD) simulations were performed using a full model for TA and truncated models (9 saccharide units) for PUL and PUL-MA (Figure S6, Supporting Information). As showcased in Figure S3, Supporting Information, the coacervate generated with PUL-MA or with the pristine form of the polysaccharide shows significant macroscopic differences. Analysis of the MD trajectories showed that the hydrophobic interactions govern the interface between TA and PUL or PUL-MA. As evidenced by the MD studies, the van der Waals energy component dominates over the other energy terms used to calculate the binding energy between the system molecules within the molecular mechanics Poisson–Boltzmann surface area (MM-PBSA) approach (**Table 1**). Besides, the introduction of the non-polar methacrylate group in the polysaccharide backbone contributed to the increase of Van der Waals forces (Table 1) between TA and PUL-MA, which led to a greater energetic stabilization of the TA|PUL-MA system when compared to the TA|PUL system.

Additionally, the average number of H-bonds established between TA, PUL, or PUL-MA, per trajectory time frame, is very small (Table 1). The results imply that most H-bond donors or acceptors in the TA, PUL, or PUL-MA molecules are establishing H-bonds with neighboring water solvent molecules. Data from the performed studies support this hypothesis since the number of H-bonds with the solvent is one order of magnitude greater than the ones observed between TA and PUL or PUL-MA (Table S2, Supporting Information). Additionally, in the most stable structures along the simulation trajectories predicted by the MM-PBSA calculations (**Figure 1**Fi–v), the OH moieties are largely oriented outward (i.e., to the solvent that is not shown) or involved in internal OH—OH bonding (intramolecular hydrogen bonding), more evident in the case of TA molecules.

Also, in the case of systems with TA, it is perceived the parallel alignment of many aromatic rings through π–π stacking for increased stability of the molecule (e.g., Figure 1Fiv). For instance, in the most stable frame for the TA|PUL-MA system (Figure 1Fii), it is also seen the stacking of methacrylate moieties of PUL-MA with the aromatic rings of TA (Figure 1Fiii). Here, the oxygen atom of the carbonyl group present in the PUL-MA methacrylic group is oriented outward, while the carbon–carbon double bond of the vinyl group is parallelly aligned through π–π stacking with the two adjacent aromatic rings of TA. Interestingly, in the case of the 1:1:4000 TA:PUL(-MA):water systems (Figures S7 and S8, Supporting Information), TA and PUL or PUL-MA moieties are positioned side by side. However, in the 2:3:4000 TA:PUL(-MA):water systems (Figure 1Fi,ii), PUL or PUL-MA fragments surround the TA molecules, suggesting a protective shield-like structure, in an attempt to reduce the number of interactions of the more hydrophobic TA species with the water solvent (Figure 1Fii). Collectively, these results demonstrate the beneficial effect of the introduction of the methacrylic group in the TA|PUL-MA system, in terms of cohesion, reinforcing the importance of hydrophobic interactions for the establishment and maintenance of coacervate systems.[33]

The analysis of the linear viscoelastic regions (LVER) of different coacervates enabled an understanding of the extent of shear strains (%) that each adhesive can withstand keeping their viscoelastic properties stable while characterizing the predominancy of elastic or viscous components in the materials. TA|PUL and TA|PUL 6% presented a predominantly viscous behavior ($G' < G''$) (Figure 1Gi,ii), with TA|PUL condition showing an LVER up to 100% deformation. On its turn, TA|PUL13% presented a more elastic behavior ($G' > G''$), with increased G' values of about 1.5 orders of magnitude when compared to the unmodified PUL-based coacervate. Additionally, the LVER limit also decreased for higher degrees of polymer modification, with 10% and 1% LVER limit strains for TA|PUL-MA 6% ($G' = 192.6 \pm 52.6$ Pa; $G'' = 452.5 \pm 81$ Pa) and TA|PUL-MA 13% ($G' = 5270 \pm 117.9$ Pa; $G'' = 4156.7 \pm 159.5$ Pa), respectively. As previously reported in the MD study, the higher number of methacrylic groups in TA|PUL-MA 13%, when compared to TA|PUL-MA 6% or the non-methacrylated counterpart, leads to an increased number of the van der Waals interactions between both adhesive components. This increase in the number of interactions between TA and PUL-MA changed the behavior of TA|PUL-MA by 13% into a solid-like material ($G' > G''$). The increased presence of methacrylic groups in the adhesives matrix also reflects their lower water uptake (Figure S9, Supporting Information) as the PUL methacrylate degree increases. Consequently, this feature outcome is an increase of the respective storage modulus (G'), resulting from the formation of a stronger cohesive network. Additionally, when compared to other commercialized adhesives, the G' values of TA|PUL-MA13% ($G' = 5270 \pm 117.9$ Pa; $G'' = 4156.7 \pm 159.5$ Pa) are higher than the characteristic values of fibrin-based adhesives ($G' = 272 \pm 7.8$ Pa; $G'' = 31.74 \pm 1$ Pa)[34] or other bioinspired adhesives reported in the literature.[35]

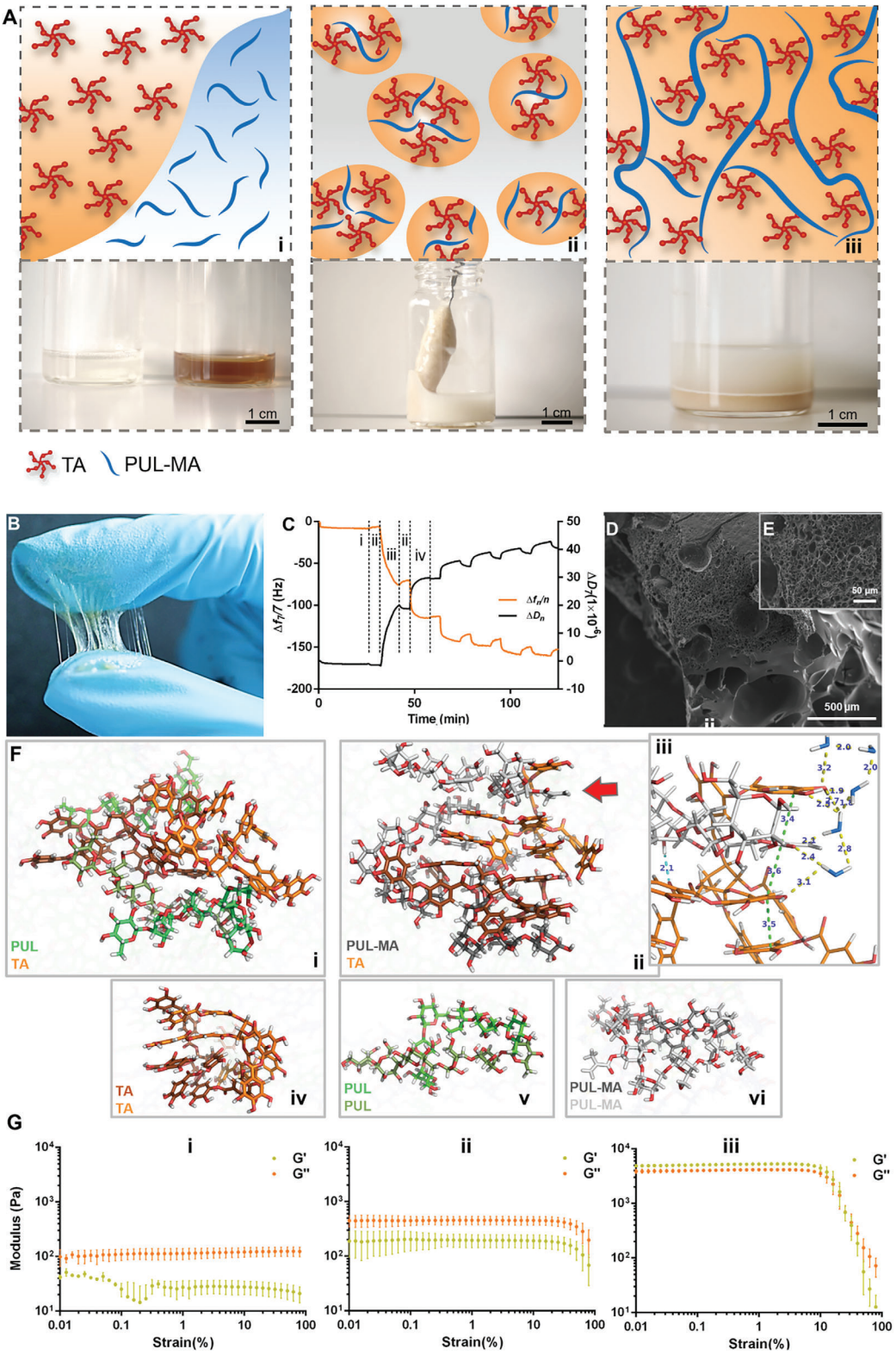

Figure 1. Characterization of TA|PUL-MA adhesives. A) Schematic representation of the molecular behavior during the formation of TA|PUL-MA adhesive together with the different process stages; i) mixture of the aqueous precursor solutions of TA and PUL-MA; ii) coacervate micelles formation after the mixture of the two solutions; iii) molecular cohesion in the dense coacervate phase and the two phases formation of the coacervate. B) Adhesion capacity of TA|PUL-MA 13% adhesive in a simple detachment test. C) QCM-D monitoring of the normalized frequency ($\Delta f_7/7$; orange line) and dissipation (ΔD_7; black line) shifts for the assessment of the build-up of TA and PUL-MA 13% bilayers via the LbL technique; the letters correspond to the adsorption of PEI

2.3. Physicochemical Characterization of the TA|PUL-MA Adhesives

Figure 1A shows the formation of the TA|PUL-MA adhesive coacervate. To further support the cross-linking mechanisms involved in the sustainment of the dense phase integrity, solid-state ^{13}C NMR (^{13}C ssNMR; Figure S10, Supporting Information) was performed on the freeze-dried TA|PUL-MA glues. The neutral polysaccharide PUL composed of maltotriose units linked by α-1,4-bonds, possesses a flexible structure, where chain flexibility depends on the ease of rotation around the anomeric links. Polysaccharide linkage through the methyl hydroxyl group exhibits heightened flexibility, owing to an additional degree of freedom in the link (ω), resulting in a trans conformation.[36] Upon combination of PUL-MA with TA, a supramolecular arrangement occurs, leading to the coacervate formation. In the ^{13}C ssNMR spectrum of TA|PUL-MA 13%, the signal assigned for 166.18 ppm (Figure S10iii1, Supporting Information) corresponds to an overlap of the resonances, both from the C═O group in the methacrylate group of PUL-MA (Figure S10ii1, Supporting Information), and the ester group (O—C═O) in TA gallol groups (Figure S10i, Supporting Information). The signal at 144.59 ppm (Figure S10iii10, Supporting Information) corresponds to the resonance of the *metha* carbons of the TA aromatic phenols. This corroborates the NMR signal observed in TA spectra, which has a resonance at 143.74 ppm (Figure S10i2, Supporting Information). This slight shift suggests that this group is involved in the little amount of hydrogen bonds holding the glue matrix. In addition, the signal at 74.12 ppm (Figure S10iii6) also corresponds to a shift of the signal at 74.29 ppm in the PUL-MA spectrum (Figure S10ii5, Supporting Information), which might indicate that the CH—OH group in PUL-MA is also involved in the establishment of the hydrogen bonds. Moreover, as demonstrated by the MD simulations, the hydrophobic interactions play a significant role in the cohesive integrity of the adhesive, leading to water removal from the interior of the adhesive matrix.[37] These results are consistent with the deviation observed in the signal of the PUL-MA spectrum at 136.01 ppm (Figure S10ii2, Supporting Information), which in the TA|PUL-MA spectrum appears at 138.28 ppm (Figure S10iii2, Supporting Information). The shifts of the signals reflect the physical nature of the bonds established between PUL-MA and TA, which do not correspond to the formation of a new structure through covalent bonds, since no new signals are observed. Besides, a deviation of the signal at 89.28 ppm in the PUL-MA spectrum (Figure S10ii6, Supporting Information) to 89.53 ppm (Figure S10iii5, Supporting Information) suggests that the methacrylic group is associated with the aforementioned hydrophobic interactions.

To provide further insights into the stability of the molecular interactions between the two molecules, TA and PUL-MA aqueous solutions were sequentially deposited through the LbL assembly technology. Figure 1C showcases the changes in the normalized frequency ($\Delta f_n/n$) and dissipation factor (ΔD_n) obtained at the seventh overtone ($n = 7$; 35 MHz) along the time during the build-up of three TA/PUL-MA bilayers onto the Au-plated quartz crystal sensor. To ensure a homogeneous surface charge density, a first positive poly(ethyleneimine) (PEI) monolayer was adsorbed onto the Au-plated quartz crystal (Figure 1Ci). Although more pronounced in the first bilayer, the sequential decrease in $\Delta f_7/7$ value after the adsorption of each of the molecule aqueous solutions proves the deposition and the effective interaction between TA and PUL-MA (Figure 1Ciii,iv). Besides, the successive increase in the ΔD_7 value reveals the viscoelasticity of the adsorbed layers, which is a typical feature of soft and hydrated polymeric materials.[38] In contrast to the traditional ionically paired polyelectrolyte multilayers widely employed to date,[39,40] the negative charge of both TA and PUL-MA aqueous solutions, previously evaluated by zeta potential (Table S3, Supporting Information), reinforces the sequential deposition of the layers predominantly stabilized by van der Waals forces.[41] In addition, the microstructure of the TA|PUL-MA adhesive was evaluated by SEM (Figure 1D,E). As can be observed, the adhesive structure shows some porosity, characteristic of TA-containing materials, since this molecule behaves not only as an adhesive moiety but also has a non-covalent crosslinker of the PUL-MA chains, thereby leading to the formation of a denser and small pore structure.

2.4. Versatility of the Administration of TA|PUL-MA Adhesive and On-Demand Detachment Triggered by UV

The delivery of the adhesive biomaterials to an intended body location can be challenging, mainly when minimally invasive delivery is preferred.[6] Injectability is an attractive feature for less complicated and quicker applications. Here, this feature was first visually evaluated (Movie S1, Supporting Information), as well as through the evaluation of the shear-thinning properties of the material (Figure S11, Supporting Information). The decrease in viscosity of the TA|PUL-MA 13% coacervate with increasing shear rate (s^{-1}) shows the ability of the biomaterial to be injected, demonstrating the required versatility to be delivered to the spot of treatment and to reverse to its original form.[42,43] **Figure 2A** also illustrates the outstanding flexibility of the natural-derived TA|PUL-MA 13% adhesive to adapt to different movements, including extensional and torsional deformations. This behavior stands out in high contrast to the mechanical response

(i), washing step with dH_2O (ii), deposition of TA (iii), adsorption of PUL-MA 13% (iv). D,E) Representative SEM images of TA|PUL-MA 13% adhesive. F) Simulations of the coacervate formation differences between TA and PUL or PUL-MA. Most stable structures found for the i) 2:3:4000 of TA:PUL:water system; ii) 2:3:4000 of TA:PUL-MA:water system (the red arrow indicates a methacrylate group of PUL-MA with its π region parallelly aligned with the aromatic rings of TA with magnification in (iii) showing selected distances in Å); iv) 2:4000 of TA:water system; v) 2:4000 of PUL:water system; and vi) 2:4000 of PUL-MA:water system. Color code: red – Oxygen; white – Hydrogen. Solvent molecules are not shown for clarity except near-neighbor contacts in (iii) with blue representing water oxygen atoms. Blue, green, and yellow dashed lines highlight an H-bond between TA and PUL-MA, distances between TA and PUL-MA π regions, and close interactions involving solvent molecules, respectively. G) Rheological characterization of the adhesive coacervates. Linear viscoelastic region (LVER) determination for i) TA|PUL 20|20, ii) TA|PUL-MA 20|20 6%, and iii) TA|PUL-MA 20|20 13%.

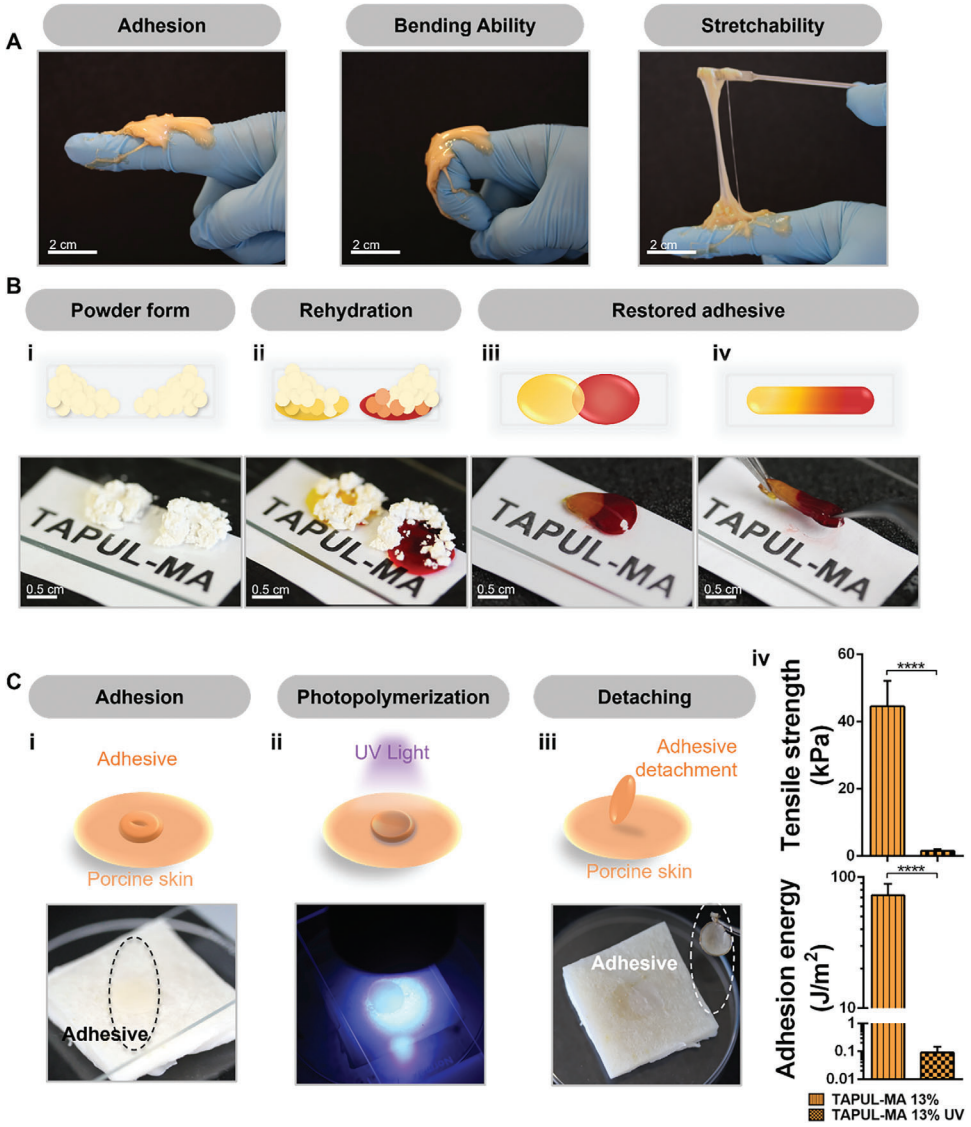

Figure 2. Attachement, detachment, and restorability properties of TA|PUL-MA. A) Demonstration of the flexibility and bonding ability of TA|PUL-MA 13% adhesive, inducing its capacity to bend and to be outstretched. B) Restorability of TA|PUL-MA adhesive; i) TA|PUL-MA 13% in powder form after freeze-drying and cryogrinding; ii) rehydration of the TA|PUL-MA 13% powder with an amount of dye according to the respective water content; iii,iv) two parts of restored adhesive after being hydrated at 37 °C for 5 min. C) Undemanding detaching of TA|PUL-MA adhesive triggered by photopolymerization; i) deposition of the adhesive on porcine skin; ii) photopolymerization; iii) easy detachment of the adhesive from the porcine skin after UV irradiation as a film; iv) comparison of tensile strength and adhesion energy of TA|PUL-MA 13% before and after UV photopolymerization.

of cyanoacrylates, which turn into a rigid and inflexible solid upon contact with water, unable to support the dynamic movements of tissues.[44]

In an attempt to have an off-the-shelf product, the adhesive coacervate was converted into powder form (Figure 2Bi). This was obtained by dehydration through lyophilization and cryogrinding. Then, two powder parts of TA|PUL-MA 13% were stained using red and yellow pigment solutions (Figure 2Bii), being able to restore their properties again (Figure 2Biii,iv and Movie S2, Supporting Information). The two separated parts of the restored material completely merged into a consistent adhesive in only 5 min. The obtained powders could be stored for more than 4 weeks and reconstituted in water on-demand to obtain the adhesive when necessary. This feature widens the application spectrum and versatility of the current adhesive biomaterial, namely by injecting the material that was just restored, or by applying it in powder form in the desired area.

Additionally, the effect of photocrosslinking the PUL-MA-based coacervates in the presence of a photoinitiator was explored as a way to enhance the cohesion of the adhesive (Figure 2C). Previous research has indicated that the improvement of the cohesion of adhesives has proven useful for their detachment as non-breaking structures, and improved adhesiveness.[45,46] Here, the photopolymerization led to the loss of adhesion capacity (1.5

± 0.5 kPa) of the material (Figure 2Civ), enabling the fast and easy removal of the TA|PUL-MA 13% adhesive, just by peeling it off from porcine skin (Figure 2Ciii and Movie S3, Supporting Information). After photopolymerization, the adhesive material suffered a decrease of 10 ± 0.9% in its weight. This is a consequence of the formation of a more intricate net in the material matrix, resulting in the release of water after UV irradiation. We hypothesize that the generation of the covalent bonds in the coacervate dense phase, which has a high polymer density, leads to molecular constraints by the entrapment of TA inside the PUL-MA matrix, and, consequently, the loss of adhesiveness. The capacity to easily remove adhesives after their application is an important feature in cases of sensitive skin or, for instance, when the application of the adhesive in the injured site is not performed accurately.[47] Therefore, we report a strategy for adhesive removal in an undemanding and painless way, without leaving any adhesive remains (Movie S3, Supporting Information).[45] From a practical perspective, if the photoinitiator activity is lost during the adhesives lifetime, a small volume can be added and allowed to diffuse through the coacervates before light-induced removal.

2.5. Self-Healing Ability of the Off-the-Shelf TA|PUL-MA Adhesives

Self-healing properties improve the life span of biomaterials after implantation when these are subjected to frequent body movements.[48] Biomaterials supported by non-covalent interactions, such as hydrophobic, electrostatic interactions, or hydrogen bonds, often demonstrate self-healing ability.[49] As such, we tested the self-healing ability of the off-the-shelf version of the developed TA|PUL-MA adhesives. Two restored parts of TA|PUL-MA 13% stained using red and blue pigment solutions were left to spontaneously merge (Movie S4, Supporting Information). The two separated parts of the restored adhesive completely merged into a consistent adhesive in only 5 min. By further stretching it, the restored adhesive behaved as a whole piece, without rupture in the color transition zone. The dynamic bonds established between TA and PUL-MA translate into the regeneration ability demonstrated by TA|PUL-MA adhesives, resulting in excellent self-healing behavior.

2.6. Tissue Adhesion Strength of TA|PUL-MA Adhesives

Although mussel-inspired approaches have been widely used as a strategy for increasing the adhesive strength in biomaterial design, the achievement of significant adhesion is usually associated with high curing times,[50] as well as the use of polymers of synthetic origin,[51] both often correlated with failure in medical translation.[52] The interfacial toughness (adhesion energy) and the tensile strength of the proposed coacervate were evaluated by the standard tensile test (ASTM F2258), and the shear strength was assessed through the lap-shear test (ASTM F2255) (**Figure 3**). Both tests were carried out on porcine skin due to its resemblance to the mechanical robustness of human skin.[53] Two formulations, with and without the addition of CATA—an enzyme introduced to the system to improve its cytocompatibility, as discussed in the following section—were assessed.

For tensile tests, TA|PUL-MA 13% presented the best performance when compared to TA|PUL and TA|PUL-MA 6%, with a tensile strength of 44.6 ± 7.6 kPa, corresponding to an adhesion energy of 72.7 ± 16.2 Jm^{-2} (Figure 3A). Although the addition of the enzyme contributed to both a decrease in the tensile strength (30.8 ± 5.6 kPa) and adhesion energy (41.7 ± 21.2 Jm^{-2}), TA|PUL-MA 13% still demonstrates higher adhesive strength than fibrin commercial adhesives (20 Jm^{-2}), for the same substrate.[4] In addition, TA|PUL-MA 13% exhibited stronger tensile strength than TA|PUL-MA 6% (28.7 ± 5.1 kPa; $^{****}p < 0.0001$), even with the incorporation of CATA (17.6 ± 3.6 kPa). This effect is associated with the higher methacrylation degree of the adhesive formulation, leading to higher cohesion and adhesion, which is also corroborated by the performance of the non-methacrylated counterpart (Figure 3). Regarding the lap-shear test, TA|PUL-MA 13% demonstrated higher adhesion performance than TA|PUL-MA 6% ($^{****}p < 0.0001$). Also, shear adhesion strength followed the same tendency showcased in the tack test, being almost threefold higher than the one reported for commercial fibrin glue.[22] The addition of the CATA enzyme led to a significant decrease ($^{****}p < 0.0001$) in the shear adhesion force of TA|PUL-MA 13%. Yet, the observed shear strength of TA|PUL-MA 13% adhesive was superior to the performance of fibrin adhesives.[54]

To evaluate the adhesion stability of TA|PUL-MA 13% adhesive in underwater conditions, the adhesive was first applied on fully wet porcine skin and then immersed in either PBS or Dulbecco's Modified Eagle's Medium-low glucose (DMEM-LG). The same replicate was tested after 24 and 72 h immersion. Figure 3Civ displays the adhesion energy (Jm^{-2}) results. No significant statistical differences were verified between either the immersion in PBS or medium and the material maintained its adhesive capacity for up to 72 h immersion in both fluids. However, the observed results for the adhesion capacity after immersion in PBS were slightly better (24 h – 75.4 ± 5.1 Jm^{-2}), when compared to the immersion in DMEM-LG (24 h – 62.6 ± 5.4 Jm^{-2}). Therefore, to better mimic real conditions, to both tissue-adhesive interfaces, blood was added before immersion in PBS (Movie S5, Supporting Information). No significant statistical differences were observed, either between timepoints or with the other two previously tested conditions. Furthermore, the results are comparable to those previously observed with humid porcine skin (Figure 3Aii, 72.7 ± 16.2 Jm^{-2}), with no statistically significant differences being noted. The results demonstrated that TA|PUL-MA 13% could glue to both skin sides, even in the presence of blood, and further full immersion in liquid media at 37 °C, showing its ability to withstand conditions close to the ones found in the human body.

Additionally, to further evaluate the adhesion capacity of our engineered adhesive, we performed several ex vivo experiments using freshly isolated organs. First, TA|PUL-MA 13% was applied to the surface of a thoroughly wetted internal oral cavity. As can be seen (Movie S6, Supporting Information), the adhesive coacervate remains adhered, even in a position susceptible to the force of gravity. Also, to test the underwater adhesion of TA|PUL-MA 13% under a more dynamic environment, a porcine intestine was filled with running water (Figure 3Cvi) and a 3 mm incision was performed. The TA|PUL-MA 13% adhesive was applied in a PDMS surface directly on the incision and could effectively seal

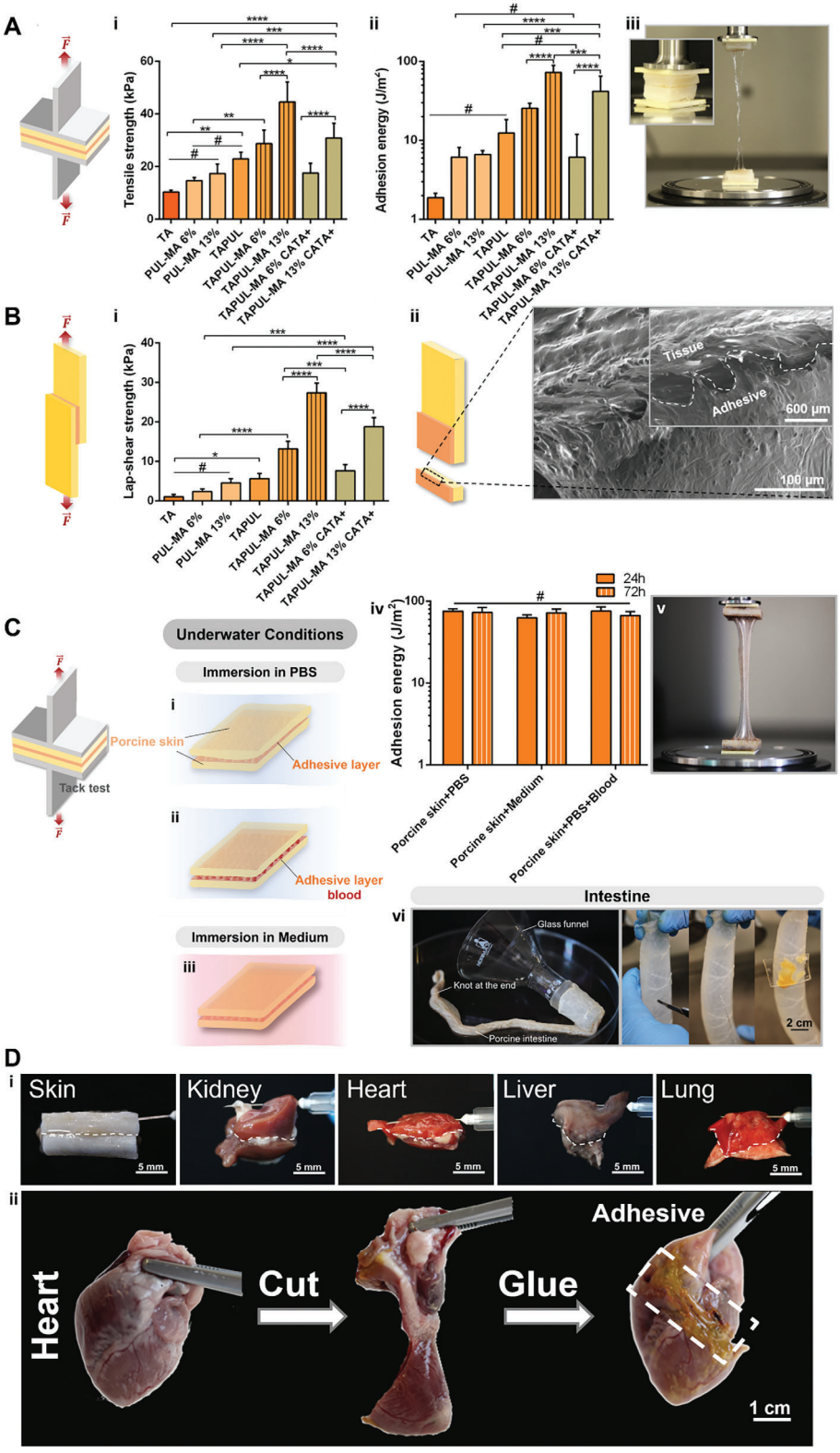

Figure 3. Adhesion properties of TA|PUL-MA adhesives. A) Representation of the setup for tensile strength measurement; i) tensile strength of the adhesives and their counterparts on porcine skin and ii) the respective adhesion energy; iii) images of the test setup immediately before and after the test. B) Representation of the setup measurement for the lap-shear test; i) shear strength of the adhesives and their counterparts on porcine skin; ii) SEM analysis of the cross-section between the porcine skin and TA|PUL-MA 13% CATA$^+$ adhesive after the lap-shear test. C) Schematic illustration of the immersion conditions in i) PBS, ii) PBS with blood, and iii) DMEM-LG, at 37 °C before tensile strength measurement; iv) adhesion energy of TA|PUL-MA

the water leakage within a few seconds of pressing (Movie S7, Supporting Information).

2.7. Cytotoxicity Assessment of the TA|PUL-MA Bioadhesives

The cytocompatibility of the TA|PUL-MA adhesives was assessed by cytotoxicity studies of the leachable contents and possible degradation products of the adhesives collected for 24 h, in contact with the L929 fibroblast cell line (**Figure 4A**). Cells cultured in the media with the degradation products of all studied coacervate formulations showed significant cell death at day 1 (Figure 4B,D; <40% viability; $p < 0.0001$ compared to control). These results support the hypothesis that molecules comprising catechol groups in its structure are cytotoxic through the generation of ROS, as previously discussed.[55] Besides, studies suggest that the excess accumulation of mitochondrial ROS leads to pyroptosis-induced inflammation and consequently cell death.[56,57] Neutral to basic pH environments result in the production of ROS, namely H_2O_2 with apparent high persistence in cell culture medium, as a by-product from the autoxidation of catechols.[12] In contrast, the extract content derived from TA|PUL-MA adhesives supplemented with CATA did not induce deleterious effects on cells, which remained viable in all adhesive formulations (Figure 4D,E; ≥90% viability) with no significant difference when compared to control samples. We hypothesize that the presence of the enzyme within the glues yielded higher cell viability due to its intrinsic capacity to degrade ROS released to the medium.

Cell metabolic activity in the presence of leachables obtained from enzyme-containing materials is maintained up to day 3 (Figure 4C,E). According to ISO 10993–5 for the biological evaluation of medical devices, a material is considered to have a cytotoxic effect if it leads to a reduction of more than 30% in cell viability, which was not verified in the present study for the adhesives incorporating CATA enzyme, showing the potential cytological safety of TA|PUL-MA adhesive.

In physiologic implantation conditions, leachables generated from biomaterials degradation are subject to removal from the body application site. Therefore, as schematically represented in Figure 4A, on day 3 the extraction media from TA|PUL-MA glues was replaced by fresh media aiming to replicate what could happen in the human body conditions. This trial was then extended to day 7. Although there is a significant difference between the viability of cells in the samples with the enzyme compared to the control sample (Figure S12, Supporting Information), the remaining surviving cells presented similar metabolic levels to day 1. This result is in opposition to the response of cells in the culture medium without the enzyme, which could not proliferate. These results indicate that the use of CATA can be a beneficial strategy to increase the survival and proliferation of cells in contact with oxidizing catechol-containing compounds.

2.8. Antibacterial Performance of TA|PUL-MA Bioadhesives

The disruption of tissue integrity opens the possibility for the entrance of pathogenic microorganisms.[58] The production of phenolic compounds by plants works often as a defense strategy against microbial infections.[59] TA is a natural antimicrobial agent thought to be present in all plant species. Its use as a component of antimicrobial biomaterials has been explored.[15] To assess the potential antibacterial capacity of the developed bioadhesives for avoiding contamination by microorganisms, appropriate infection models of *Staphylococcus aureus* and *Escherichia coli* were chosen as representative Gram-positive and Gram-negative bacteria, respectively. *S. aureus* is a common gram-positive pathogenic bacterium responsible for numerous infections due to being one of the super antibiotic-resistant microorganisms.[60] In other clinical cases, other strains of bacteria, such as the anaerobe *E. coli*, can be present and intensify the extent of the infection. Growth inhibition assays in agar diffusion discs were performed with TA|PUL-MA adhesive samples, using TA as a positive control, since it is a well-studied antimicrobial agent.[61,62] The results show significant inhibition zones for both adhesive formulations with both strains of bacteria (Figure S13, Supporting Information), demonstrating the outstanding antibacterial potential of TA|PUL-MA adhesives. As expected, TA avoided the proliferation of both types of microorganisms, but it is worth noting that the antibacterial activity of the polyphenol compound was stronger against *S. aureus* (Figure S13C,D, Supporting Information). The same trend was followed by the two adhesive formulations. Besides, no significant differences between TA and each of the TA|PUL-MA adhesives within the same bacterial strain were denoted. This demonstrates that, despite its interaction with the polysaccharide, TA has the same antibacterial capacity compared to its standalone form.

TA|PUL-MA adhesives embodying the CATA enzyme were tested for the maintenance of the antimicrobial capacity. **Figure 5** showcases evident inhibition halos in all samples with both strains, with and without the enzyme. Although the presence of CATA reduced the antibacterial capacity (Figure 5B,C, Supporting Information), the adhesives were still able to inhibit bacteria proliferation. Although the exact antibacterial mechanism of TA is not entirely described, catechol groups can cause deleterious and irreparable effects in cells, by the capacity to directly react with a wide range of biomolecules (e.g., lipid peroxidation, enzyme inactivation, DNA strand breaks, or adduct formation), or through their redox chemistry. The oxidation of catechol groups is followed by the production of ROS (e.g., O_2^-, H_2O_2, OH) which, depending on the amount in which they are present, are hazardous for cells.[63,64] Therefore, considering that a plausible explanation for the antimicrobial effects relies on the localized generation of ROS-rich environments, it is interesting to observe that the amount of CATA added to the adhesives was enough to ensure the viability of cells (see Section 2.7), without

13% adhesive on porcine skin after 24 and 72 h immersion on either PBS, PBS with blood, or DMEM-LG; v) image of the test setup immediately after the test; vi) (left) structure built for underwater and under pressure adhesion testing of TA|PUL-MA 13% in porcine intestine; (right) application of the adhesive on a 3 mm incision of the intestine. D) Optical images of TA|PUL-MA 13% adhering to i) porcine skin and some of the main rabbit tissues (kidney, heart, liver, and lung); ii) photographs of TA|PUL-MA 13% adhesive applied in a rabbit heart that was cut in two pieces, as an example of adhesion in static conditions. # – no statistical differences were identified, $^{**}p < 0.01$, $^{***}p < 0.001$, $^{****}p < 0.0001$).

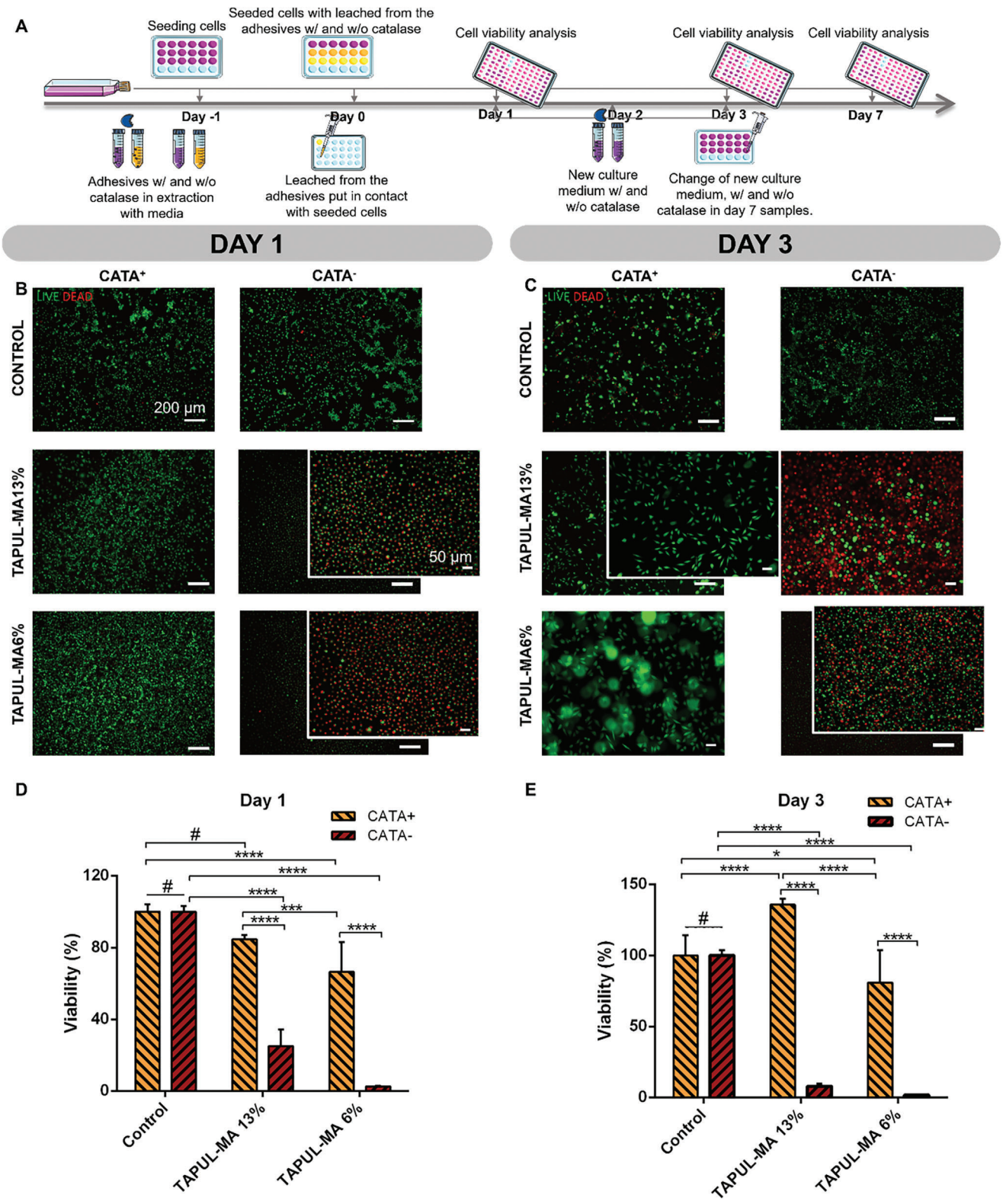

Figure 4. Evaluation of the cytotoxicity of the TA|PUL-MA adhesives with and without CATA enzyme. A) Schematic representation of the experimental design of the assay. Representative fluorescence microscopy images of live-dead assay of L929 cells cultured with the extracted products from the adhesives with and without CATA enzyme B) for day 1 and C) for day 3. Metabolic activity of L929 cell line at D) 1 day and E) 3 days of culture with the derived products from the glues. *$p < 0.05$, ***$p < 0.001$, ****$p < 0.0001$, # – no statistical differences were identified.

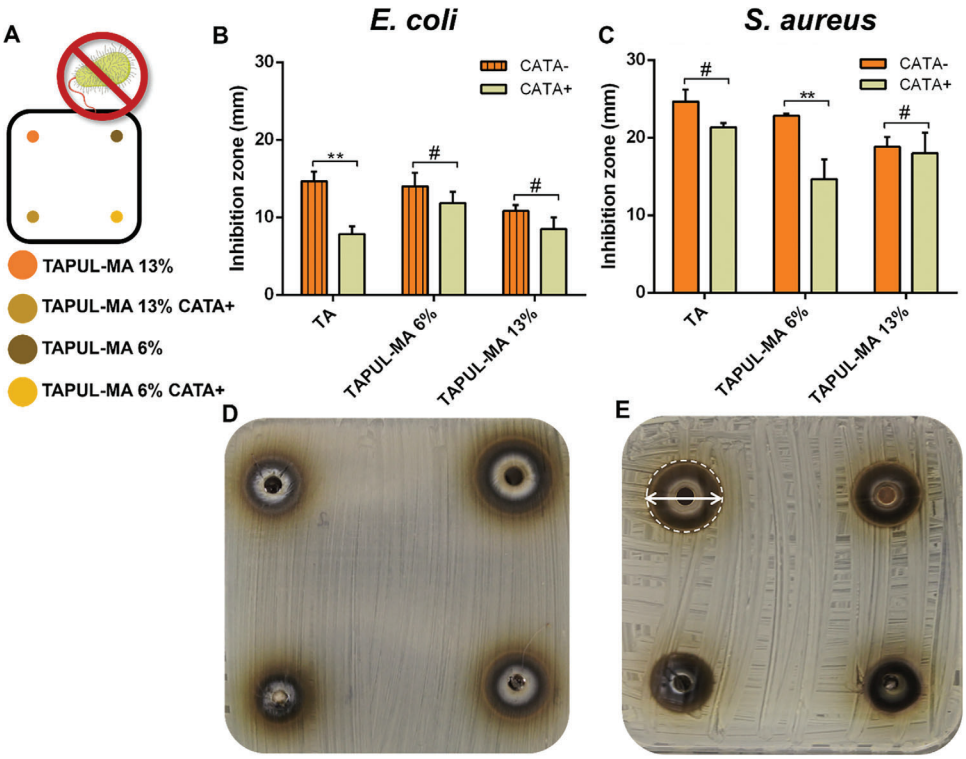

Figure 5. In vitro assessment of the antibacterial properties of TA|PUL-MA adhesives against gram-negative *Escherichia coli* and gram-positive *Staphylococcus aureus*. A) Schematic representation of the distribution of the different samples on the test plate. Size of the inhibition zone (mm) of each of the TA|PUL-MA adhesives and TA with and without CATA enzyme for B) *E. coli* and for C) *S. aureus*. D) Antibiogram of *E. coli*. E) Antibiogram of *S. Aureus*, where the signalized area represents one of the inhibition halos. Bars indicate mean ± standard deviation. ** $p < 0.01$, $n = 4$ samples for all groups.

compromising their antibacterial activity. In the case of TA, the observed differences with and without the enzyme verified for *E. coli* might be due to the scavenging of ROS by the enzyme. Regarding the adhesives, as previously described, the antibacterial activity is superior against *S. aureus*. Though, the blocking effect of CATA is more significant in the case of TA|PUL-MA 6%, decreasing its antibacterial potential. The viscosity of TA|PUL-MA 6% is lower than TA|PUL-MA 13% (Figure 5C) due to its lower methacrylation degree, allowing free interaction of the enzyme with its substrate or, an easier release of the enzyme into the medium. Thus, the observed scavenging effect is more significant, which also explains the higher antibacterial effect of TA|PUL-MA 6% when the enzyme is absent.

2.9. In Vitro Hemostatic Performance and Burst Pressure Characterization of TA|PUL-MA Bioadhesives

During surgical procedures or trauma, hemorrhages may occur when serious lesions happen. Therefore, the hemostatic ability may be an important feature in the design of bioadhesives. TA|PUL-MA adhesives were evaluated through the blood clotting test, assessing the time for the formation of the blood clot in whole blood when in contact with the adhesives and their counterparts. In the human body, normal blood clotting is reported to be between 5 and 10 min.[65] However, citrated whole blood handled in silicone-treated tubes has a very long clotting time,[66] namely between 19 and 60 min.[67] This tendency was observed in this study, where, after the addition of $CaCl_2$, the control blood took 26.7 ± 5 min to coagulate (**Figure 6**). The blood exposure to TA led to a much quicker blood coagulation time (4.1 ± 0.02 min). Polyphenols are reported to accelerate blood coagulation, by triggering a clotting cascade due to the activation of coagulation factor XII by their negative charge.[68–70] In contrast, PUL-MA 6% and PUL-MA 13% kept the red color of the blood, similar to the control sample, showing weak blood clotting abilities (Figure 6A).[71] The hemostatic capacity of TA was maintained in TA|PUL-MA 13% (6.1 ± 2.2 min) and TA|PUL-MA 6% (5.1 ± 2.9 min) adhesives even with CATA enzyme, and it was significantly higher than the control (****$p < 0.0001$).

When in contact with blood, new medical biomaterials should not only promote the formation of the blood clot but also be hemocompatible, a property commonly evaluated by the hemolysis ratio (%). For the use of biomaterials in blood-associated applications and according to the ASTM, the reported hemolysis limit corresponds to 5%.[72,73] Although, it is worth noting that certain authors have suggested that a hemolysis rate of 2% or less is considered the benchmark of best practice.[74] As showcased in Figure 6B, there were no significant differences between triton-X and its counterpart with $CATA^+$, thus the comparison was made relative to simple triton-X. As observed, the two TA|PUL-MA adhesives with CATA enzyme (Figure 6B; TA|PUL-MA 13% $CATA^+$ and TA|PUL-MA 6% $CATA^+$) are easily distinguished from the triton-X samples (positive control) (****$p < 0.0001$) and their correspondent hemolysis ratio is lower than the established limit of 5% for biomaterials, and therefore they are hemocompatible

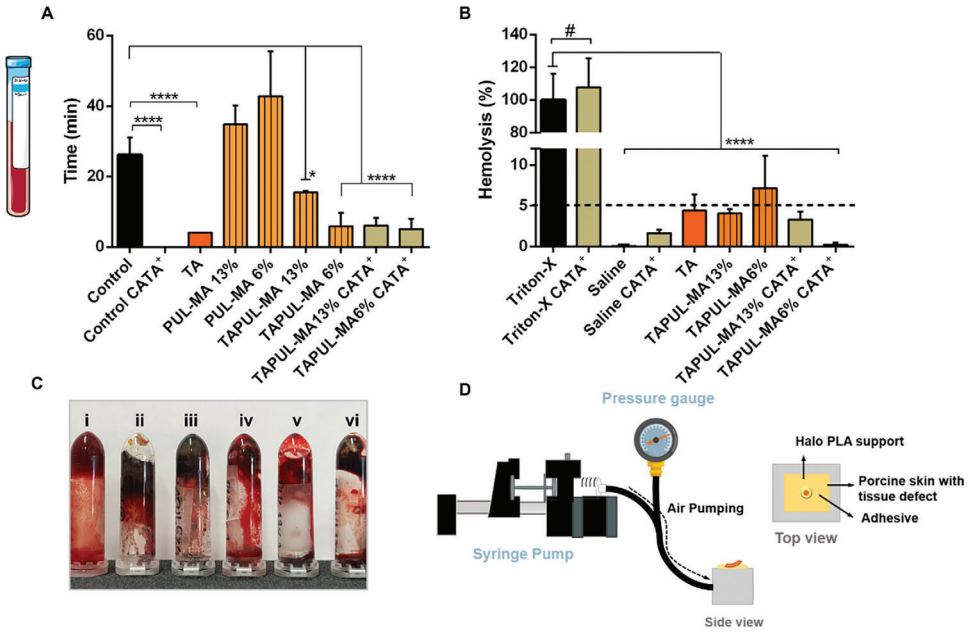

Figure 6. In vitro blood compatibility evaluation assays. A) Clot formation with the adhesives as a function of time (min) in blood clot test with human blood; B) Hemolysis percentage calculated according to Equation (3) of red blood cells in contact, for 1 h at 37 °C, with TA|PUL-MA adhesives and its counterparts; C) TA|PUL-MA adhesives and its counterparts in contact with human blood in the blood clot test. i) Control, ii) TA, iii) TA|PUL-MA 6%, iv) PUL-MA 6%, v) PUL-MA 13%, and vi) TA|PUL-MA 13%. D) Schematic representation of the device used for the evaluation of the burst pressure (Movie S8, Supporting Information).

for medical use. Although fibrin sealants are effective hemostatic agents, their animal origin poses the possibility of viral contamination, bacterial infection, and immunogenicity,[75] and they lack strong adhesive properties. Therefore, the aforementioned features reinforce the possible use of TA|PUL-MA as a potential medical adhesive.

Besides a positive interaction with blood and the promotion of the blood clot, another strategy is to use medical adhesives to physically block the bleeding site.[76] In this regard, depending on the desired final application, a medical adhesive must withstand pressure values equivalent to normal arterial blood pressure (<120 mmHg).[77] TA|PUL-MA 13% adhesive was tested ex vivo regarding its ability to avoid air leakage, using a porcine skin model. The adhesive capacity of the material allowed it to withstand a pressure of 150 mmHg (Movie S8, Supporting Information), greater than normal blood pressure. Fibrin is reported to sustain a pressure equivalent to 24.75 mmHg,[34] making it evident that the present adhesive demonstrated a better performance than the current fibrin adhesives. This demonstrates that TA|PUL-MA adhesive can tightly bind to the wound tissues and effectively act as both a barrier and a hemostatic agent.

2.10. Benchmarking of the Developed Adhesive with Literature and Commercially Available Counterparts

The production of ROS is believed to be accountable for the antibacterial capacity of catechol-containing adhesives. However, the presence of these groups is also responsible for decreasing their biocompatibility.[12,78] Several strategies, such as metal-ion coordination, enzymatic crosslinking,[10] or self-polymerization upon oxidation,[35] have been employed in the design of the biomaterials to avoid the free oxidation of the catechol groups. Although these fabrication approaches increase substantially the cytocompatibility, the materials usually present low adhesive capacity and end up with almost no antimicrobial properties.[79] Regarding the latter, Table S4, Supporting Information, summarizes representative literature examples of mussel-inspired adhesives manufactured through circumvention strategies consisting in the addition of cationic moieties,[51] silver ions (Ag^+), and silver nanoparticles (AgNPs),[15] or other metal ions and particles.[16] These approaches are also responsible for endowing adhesives with antimicrobial capacity.

Figure 7 shows a benchmarking evaluation of TA|PUL-MA adhesive in comparison with representative literature examples of adhesives based on catechol chemistry, as well as widely employed commercially available adhesives. The information is based on information gathered in Table S5, Supporting Information. Aspects concerning adhesion strength, cytocompatibility, hemostatic properties, antibacterial activity, and curing time are compared. Synthetic-based adhesives usually combine high adhesion capacity with long curing times and also exhibit antibacterial activity. Adhesives derived from natural molecules usually show lower adhesion strengths, while showing a more evident balance between all analyzed properties. The same can be seen in adhesives that are already commercialized, where fibrin adhesives, despite having weak adhesive capacity, show concomitant cytocompatibility and hemostatic capacity. In contrast, although the adhesive capacity of cyanoacrylates is widely known, their toxicity is a major drawback that restricts them to topical applications. The adhesive system presented here was able to combine multifunctional features, namely concomitant cytocompatibility

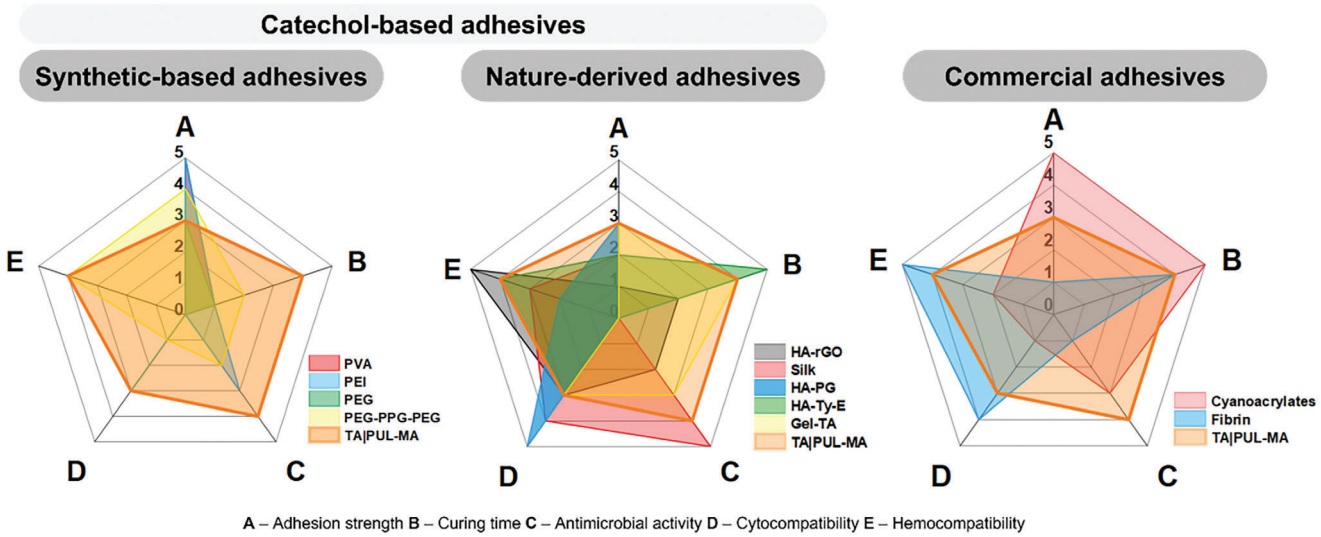

Figure 7. Benchmarking study of TA|PUL-MA 13% adhesive with other literature catechol-based adhesives and commercially available adhesives. Assessment performed with information available in Tables S4 and S5, Supporting Information.

and natural antibacterial activity, along with hemostatic capacity and improved adhesion strength in comparison to commercially available fibrin sealants, presenting a compromise between all the properties in the same formulation.

3. Conclusion

Here, a natural-derived TA|PUL-MA adhesive was produced through an entirely supramolecular, straightforward, and cost-effective methodology, by simply mixing tannic acid with pullulan methacrylate. Besides its role in the stabilization of the coacervate and further improvement of adhesive properties in porcine skin, the exploration of PUL methacrylation also enabled the photocrosslinking-triggered easy removal of the adhesives, making the strategy very appealing for applications in sensitive skin.

Rheological studies indicated the viscoelastic nature of the material ($G' \approx G''$) and the possibility to be injectable, as demonstrated by the shear-thinning properties. Without employing covalent strategies, TA|PUL-MA adhesives showed good cytocompatibility, through the introduction of a ROS-degrading enzyme—CATA—which did not compromise the excellent antibacterial activity against strains of *S. aureus* and *E. coli*. Also, the adhesives showed advantageous hemostatic ability with the shortest clotting time, and a correspondent safe hemolysis percentage ratio (>5%). Ex vivo adhesion studies revealed that the TA|PUL-MA 13% formulation denoted the best adhesive performance (44.6 ± 7.6 kPa, 72.7 ± 16.2 Jm^{-2}), even until 72 h in similar conditions to the physiological ones (72.8 ± 10.9 Jm^{-2}). Although the introduction of CATA slightly decreased both the adhesion strength (30.8 ± 5.6 kPa) and the adhesion energy (41.7 ± 21.2 Jm^{-2}), TA|PUL-MA 13% stands out as having superior adhesion strength when compared to most non-cyanoacrylate medical adhesives available commercially. Future work envisions the development of a strategy for achieving a sustained delivery of CATA, without compromising the adhesion strength of the final biomaterial to explore the clinical application of the developed adhesive.

4. Experimental Section

Materials: TA, dimethyl sulfoxide (DMSO, ≥99.5%), hydrochloric acid 37% (v/v) (HCl), DMEM-LG, and Triton X-100 were purchased from Merck (Darmstadt, Germany). Spectra/Por 1 dialysis tubing with a molecular weight cut-off (MWCO) of 6–8 kDa was obtained from Repligen (Waltham, USA). PUL was acquired from Carbosynth (Berkshire, UK). 4-Dimethylaminopyridine (DMAP) was purchased from Acros Organics (Geel – Belgium). Glycidyl methacrylate and deuterium oxide (99.8%) (D_2O) were obtained from TCI Chemicals (Zwijndrecht, Belgium). Dulbecco's phosphate-buffered saline (DPBS) powder without calcium/magnesium for cell culture was obtained from Corning (Arizona, USA). Trypsin–EDTA, antibiotic/antimycotic, and fetal bovine serum (FBS) were purchased from Thermo Fisher Scientific (Waltham, MA, USA). Sodium chloride (NaCl) was obtained from LabChem (Lisbon, Portugal).

Assessment of Coacervate Formation between TA and Natural-Derived Polymers: For the assessment of the two separate phases' formation between TA and natural-derived polymers, several polysaccharide aqueous solutions were prepared according to their corresponding solubility (Table S1, Supporting Information). Each polysaccharide was mixed with a TA aqueous solution twofold the concentration of the respective polysaccharide (e.g., 10% w/w PUL + 20% w/w TA). After 24 h, the mixtures were inspected regarding the formation of coacervates.

Synthesis of PUL-MA: The methacrylation of PUL was performed according to a synthetic route already established in the group with slight modifications, based on the chemical modification of the primary hydroxyl groups present in the PUL backbone and the reactivity of the epoxy group in glycidyl methacrylate.[80] Briefly, PUL (3 g) was dissolved in DMSO (35 mL) under a N_2 atmosphere. DMAP was added (300 or 600 mg) to this solution, and then, glycidyl methacrylate (600 or 1200 µL) was incorporated to synthesize PUL-MA with low or high methacrylation degree, respectively. The mixtures were stirred at room temperature (RT), for 48 h, and then, the reaction was stopped by adding an equimolar amount of concentrated HCl solution to neutralize DMAP. The PUL-MA solutions were purified by 5-day dialysis (water change twice a day) against distilled water. The final product was obtained by lyophilization and stored in a dry place protected from light. The chemical modification of PUL was confirmed by ATR-FTIR and ^{1}H-NMR spectroscopy. The methacrylation degree was

quantified by ^{1}H-NMR spectroscopy by comparing the integrated intensity of the double bond signals of the methacrylic moieties to the one of the PUL backbone, following Equation (1)[81]

$$\text{MD}\ (\%) = 100 \times \frac{(7\ I_{\text{MA}})}{(5\ I_{\text{PUL}})} \quad (1)$$

where I_{MA} is the integral corresponding to all the protons from methacrylic moieties (1.95, 5.79, and 6.22 ppm) and I_{PUL} is the integral of all PUL protons (3.42–4.03, 4.93, and 5.34–5.39 ppm).

PUL-MA with low methacrylation degree (PUL-MA 6%) – ^{1}H NMR (300 MHz, D_2O): δ (ppm) 6.20 (s, 1H, C = CH_2), 5.78 (s, 1H, C = CH_2), 5.36 (dd, 9H, J = 10.8, 3.5 Hz, PUL backbone), 4,94 (d, 6H, J = 3.5 Hz, PUL backbone), 4.03–3.41 (m, 98H, PUL backbone), 1.95 (s, 3H, CH_3). ATR-FTIR: ν(cm^{-1}), (C—O—C) 1080, (C=C) 1637, (C=O) 1705.

PUL-MA with high methacrylation degree (PUL-MA 13%) – ^{1}H NMR (300 MHz, D_2O): δ (ppm) 6.22 (s, 1H, C=CH_2), 5.78 (s, 1H, C=CH_2), 5.37 (dd, 5H, J = 10.8, 3.5 Hz, PUL backbone), 4,93 (d, 3H, J = 3.5 Hz, PUL backbone), 4.03–3.42 (m, 47H, PUL backbone), 1.95 (s, 3H, CH_3). ATR-FTIR: ν(cm^{-1}), (C—O—C) 1080, (C=C) 1639, (C=O) 1705.

Liquid and Solid-State NMR Spectroscopy: Liquid ^{1}H-NMR spectra of PUL-MA with different methacrylation degrees were recorded using a Bruker Avance 300 spectrometer (Bruker, Germany) at 300.13 MHz, using D_2O as an internal reference. The chemical shifts are expressed in δ (ppm) and the coupling constants (J) in Hz.

^{13}C Solid-state nuclear magnetic resonance (^{13}C ssNMR) spectra of TA, PUL-MA, and TA|PUL-MA were recorded on a Bruker Avance-400 MHz spectrometer (Bruker, Germany), operating at B0 fields of 9.4 T and recorded on a triple-resonance 4, and equipped with a 4 mm Bruker MAS probe. The samples were packed into ZrO_2 rotors with Kel-F (4 mm).

The deconvolution and simulation of the NMR spectra were carried out using the program MestreNova and the chemical shifts are reported in δ (ppm).

13C ssNMR: TA – ^{13}C ssNMR (400 MHz): δ (ppm) 166.22 (O—C=O TA), 143.74 (C=C *metha*), 138.03 (C=C *para*), 118.83 (C=C *ortho*), 110.63 (C-aromatic), 93.03 (CH_2), 72.30 (—C—OH).

PUL-MA 13% – ^{13}C ssNMR (400 MHz): δ (ppm) 168.90 (O—C=O methacrylate group), 136.01 (C=C methacrylate group), 127.62 (C=CH_2 methacrylate group), 103.46 (O—C—O PUL chain), 89.28 (CH_2—O—), 74.29 (CH—OH PUL chain), 62.36 (CH_2—OH PUL chain), 18.56 (CH_3 methacrylate group).

TA|PUL-MA 13% – ^{13}C ssNMR (400 MHz): δ (ppm) 166.18 (O—C=O TA+PUL-MA), 144.59 (C=C *metha* TA), 138.28 (C=C *para* TA + C=C methacrylate group), 127.81 (C=CH_2 methacrylate group), 119.18 (C=C *ortho* TA), 111.10 (C-aromatic TA), 103.37 (O—C—O PUL-MA), 89.53 (CH_2—O—methacrylate), 74.12 (CH—OH PUL-MA), 61.95 (CH_2—OH PUL-MA), 16.80 (CH_3 methacrylate group).

Attenuated Total Reflectance-Fourier Transform Infrared: ATR-FTIR spectra were collected on freeze-dried samples by using a Mattsson 7000 galaxy series spectrometer (Mattsson, USA) at RT. Air was used as a background control, and sample spectra were recorded at a 4 cm^{-1} resolution with a total of 256 scans in the spectral region of 4000–350 cm^{-1}.

ATR-FTIR: TA|PUL-MA 6% – ATR-FTIR: ν(cm^{-1}) (C—O—C) 1078, (C=C) 1610, (H—C=O) 1707. TA|PUL-MA 13% – ATR-FTIR: ν(cm^{-1}) (C—O—C) 1078, (C=C) 1610, (H—C=O) 1707.

Freeze-Dryer: The freeze-dried products were obtained using a LyoQuest Plus Freeze-dryer (Telstar, Terrasa, Spain) at −90 °C, 96 h, and under a pressure of 0.001 mbar.

Preparation of TA|PUL-MA Adhesives: For the preparation of TA|PUL-MA adhesives, a 20% (w/w) TA aqueous solution was mixed with 20% (w/w) PUL-MA, 13% or 6% methacrylation degree, aqueous solution. The mixture was allowed to stabilize for 24 h to enable the formation of two phases. Afterward, the dense phase was recovered through centrifugation (20 min; 937 g), and the supernatant was discarded. A washing step with PBS was followed by the recovery of the coacervate dense phase. The bioadhesives were then frozen (−80 °C) and freeze-dried for subsequent characterization and recovery studies.

Computer Simulations of the Molecular System: MD simulations were carried out with GROMACS version 2019.3.[82,83] The simulation protocol comprised an initial energy minimization with the steepest descent algorithm, followed by a 1000 ps NVT simulation at 298.15 K to equilibrate the energy, a 1000 ps NPT simulation at 298.15 K and 1 bar to equilibrate the density, and finally a 100 000 ps NPT simulation at 298.15 K and 1 bar. A time step of 2 fs was considered in the integration of Newton's equations of motion with a leap-frog algorithm. The V-rescale thermostat with a time constant of 0.1 ps was used to control the temperature. The Parrinello–Rahman barostat with a time constant of 2 and isothermal compressibility of 4.5×10^{-5} bar^{-1} was used to control the pressure. The LINCS algorithm was used to constrain all bonds with H atoms. Neighbor searching considered the Verlet scheme. Cut-off radii of 1.2 nm were employed for van der Waals and electrostatic interactions. Long-range dispersion corrections for energy and pressure were applied. Long-range electrostatic interactions were calculated using PME[84] with the Fourier spacing default value of 0.12 nm.

All simulations considered cubic boxes with randomly inserted 0:2:4000, 2:0:4000, 1:1:4000, or 2:3:4000 TA:PUL:water or TA:PUL-MA:water molecules. The AnteChamber Python Parser interfacE (ACPYPE) v. 2022.1.3 script was used to automatically generate topologies within the General Amber Force Field (GAFF)[85,86] for TA, PUL, and PUL-MA from their corresponding structures in PDB format. The SPC/E model was used for water.[87]

The trajectories from the MD simulations were analyzed with the GROMACS tools (e.g., gmx hbond), and additional calculations with the MM-PBSA approach were calculated with the g_mmpbsa code.[88,89]

Quartz Crystal Microbalance with Dissipation Monitoring (QCM-D): The successful interaction between either PUL-MA 13% or PUL-MA 6% with TA was monitored in situ by the fully automated QCM-D apparatus (QSense Pro, Biolin Scientific, Gothenburg, Sweden). Before performing the experiment, gold (Au)-coated 5 MHz AT-cut quartz crystal sensors (QSX301 Gold, Q-Sense, Sweden) were submitted to UV/ozone treatment (UV/Ozone ProCleaner 220, BioForce Nanosciences, Inc.) for 10 min, and thoroughly cleaned by immersion in an oxidizing cleaning solution encompassing a 1:1:5 (v/v) mixture of NH_4OH (25%), H_2O_2 (30%), and ultrapure water in an ultrasonic bath at 70 °C, for 10 min. The substrates were then thoroughly rinsed with ultrapure water, dried under a soft stream of N_2, and resubmitted to UV/ozone treatment for 10 min. The freshly cleaned quartz sensors were introduced in the QCM-D apparatus and equilibrated in ultrapure water until reaching a baseline. To ensure a homogeneous deposition of the TA and PUL-MA layers, the quartz sensors were first exposed to a 0.5 mg mL^{-1} PEI solution (10 min adsorption time). After a washing step in ultrapure water (5 min), the Au-plated quartz sensors were alternately exposed to a 0.5 mg mL^{-1} TA (10 min adsorption time) and either 0.5 mg mL^{-1} PUL-MA 13% or PUL-MA 6% methacrylation degree (10 min adsorption time) in ultrapure water. In between the deposition of the biopolymeric materials, the substrates were rinsed with ultrapure water for 5 min to remove loosely adsorbed molecules. The assembly cycle was repeated three times, leading to PEI/$(TA/PUL\text{-}MA)_3$ multilayered thin films. To prove the successful deposition and interaction between TA and either PUL-MA 13% or 6%, the same procedure was carried out either only with TA or PUL-MA solutions (control). All experiments were performed at a constant flow rate of 50 µL min^{-1} and 25 °C. The quartz sensors were excited at multiple overtones (1, 3, 5, 7, 9, and 11 corresponding to 5, 15, 25, 35, 45, and 55 MHz, respectively) and the changes in the frequency (Δf) and dissipation (ΔD) were monitored in real-time. The frequency of each overtone was normalized to the fundamental resonant frequency (5 MHz) of the quartz crystal substrate ($\Delta f_n/n$, n denotes the overtone number). The results presented herein correspond to the frequency and energy dissipation shifts associated with the seventh overtone (n = 7; 35 MHz) owing to their lowest level of noise. However, the results are representative of the other overtones.

TA|PUL-MA Adhesives Water Content: TA|PUL-MA adhesives 20|20 (13% or 6% methacrylation degree) were made in triplicate (n = 4) and the water content (%) was measured by weighing a small portion of the coacervate, wet weight (w_w), which was then frozen and freeze-dried.

Afterward, the dry weight (w_d) was measured and compared with the initial wet weight (w_w) for water content calculation, according to Equation (2)

$$\text{Water content } (\%) = \frac{w_w - w_d}{w_w} \times 100\% \quad (2)$$

Self-Healing Ability of TA|PUL-MA Adhesives: For the evaluation of the self-healing capacity of the adhesives, after freeze-drying the adhesives were frozen (−80 °C) and processed in a cryogenic grinder (SPEX sample Prep 6775) for the generation of a powder. For the reestablishment of the adhesives, two separated amounts of each adhesive were restored with an amount of dye according to the water content for each TA|PUL-MA adhesive assessed in the previously described "*TA|PUL-MA adhesives water content*" experiment and allowed to merge for 5 min at 37 °C, for assessing their integrity.

SEM Characterization of TA|PUL-MA Adhesives: The morphology of the freeze-dried TA|PUL-MA adhesives was determined by SEM (SEM Hitachi, SU-70 instrument, accelerating voltage 15 kV, Japan) after carbon sputtering (K950X Turbo-Pumped Carbon Evaporator).

Rheological Studies of TA|PUL-MA Adhesives: Rheology was used to evaluate the developed systems regarding their LVER for characterization and strength determination, and for the assessment of their injectability, assessed through the shear-thinning behavior of TA|PUL-MA 20|20 13% and TA|PUL-MA 20|20 6%. The rheological measurements were collected using a Kinexus Pro+ Rheometer (Malvern Panalytical, UK) at 25 °C, in the case of the LVER determination, and at 37 °C for the assessment of injectability, using a stainless-steel parallel plate geometry (8 cm) and a fixed gap of 1 mm height. A shear rate range from 0.1 to 100 s^{-1} was used for the assessment of shear-thinning behavior, with a frequency of 1 Hz.

Ex Vivo Lap-Shear Adhesion Test: Adhesion to tissues of the produced adhesives was evaluated through a lap shear test according to the American Society for Testing and Materials standard protocol (ASTM F2255) with slight modifications. This test was carried out using an Instron Universal Mechanical Testing Machine 3343 (Instron, USA) equipped with a load cell of 50 N. Shortly, pieces of porcine skin (40 mm × 10 mm × 3 mm) size were prepared. After that, 50 µL of the glues (TA|PUL-MA 20|20 13% and 6%) or their counterparts (TA, PUL-MA 13% and PUL-MA 6%) were applied between two porcine skin pieces and 20 min of curing time at 37 °C were applied to evaluate the fully potential of the adhesives. The porcine skin pieces were clamped in the tensile machine and a test rate of 5 mm min^{-1} was applied. The adhesion strength (kPa) was calculated by the ratio of the load (N) and bonding area (m^2) and five samples ($n = 5$) of each group were tested.

Ex Vivo Tensile Adhesion Tests: Adhesion to porcine skin was also tested according to ASTM F2258, namely the tack test. These tests were carried out in a Kinexus Pro+ rheometer (Malvern Panalytical, UK) by recording the detachment stress of the TA|PUL-MA adhesives between a probe and a base plate, each of them covered with a piece of porcine skin (0.01 × 0.01 m^2; $n = 6$). The adhesion strength of the adhesives was evaluated with and without catalase (CATA). After sample application (50 µL), a 20 min contact time was set before pulling the two parts at a speed of 0.5 mm s^{-1}. To assess the tensile adhesion strength, the maximum peak force was divided by the skin bonding area where the glue was applied. To assess the adhesion energy value (Jm^{-2}), the area under the curve of force (N) versus displacement (mm) was assessed. For the assessment of the underwater adhesion, the TA|PUL-MA 13% adhesive was applied onto porcine skin, with and without exposure to fresh human blood (100 µL) on the skin surface. Then, a 20-min contact period with a weight (50 g) was performed at 37 °C. Afterward, the two glued pieces were immersed, either in PBS or DMEM-LG, and left in an oven at 37 °C for 24 and 72 h. At the determined timepoints (24 and 72 h), the samples (0.015 × 0.015 m^2; $n = 6$) were analyzed for the assessment of the adhesion energy. Before pulling the two skin parts, a 10-min contact time in the rheometer was set. After debonding, the two porcine skin surfaces were glued again with the remained adhesive for evaluating the adhesion energy after 72 h immersion in PBS or DMEM-LG. To assess the adhesion energy value, the area under the curve of force (N) versus displacement (mm) was assessed, and the force was divided by the skin area where the glue was applied.

Ex Vivo Experiments Using Freshly Isolated Organs: Part of a porcine intestine was recovered from the slaughterhouse. One side was connected to a funnel so water could easily flow inside the intestine. On the other side, a knot was tied to avoid any leakage. When the intestine was completely filled with water, a ≈3 mm long incision was introduced with a scalpel to induce a leakage. Since this ex vivo test only required one side of the bioadhesive, TA|PUL-MA 13% adhesive was then applied to the incision area, during 20 s pressure application, with the opposite surface covered with a PDMS sheet to permit sufficient pressure application without adhering to the applicator's glove.

TA|PUL-MA Adhesive and Porcine Skin Cross-Section Analysis: After the lap-shear test, the cross-section of the adhesive-porcine tissue surface was fixed in 4% (w/v) formaldehyde, and then dehydrated in an increasing gradient series of ethanol. The samples were fixed in a stub with the cross-section visible. After carbon sputtering (K950X Turbo-Pumped Carbon Evaporator), the morphology of the adhesion surface was visualized by SEM (SEM Hitachi, SU-70 instrument, Japan) at an accelerating voltage of 15 kV.

On-Demand Detachment Triggered by UV: Adhesion capacity after photopolymerization was also tested according to ASTM F2258, namely the tack test. This was carried out in a Kinexus Lab+ rheometer (Malvern Panalytical, UK), equipped with a UV curing accessory, by recording the detachment stress of the TA|PUL-MA adhesives (50 µL) between the probe and the base plate ($n = 6$). After sample application, UV irradiation (0.95 W cm^{-2}) for 60 s was set before pulling the two parts at a speed of 0.5 mm s^{-1}. To assess the adhesion strength, the maximum peak force was divided by the skin area where the glue was applied. Tests were performed at 25 °C.

Preparation of the Bioadhesives Liquid Extracts and Assay Methodology: The indirect test contact was performed according to ISO 10993–5 (2009) for the biological evaluation of medical devices – Part 5: Tests for in vitro cytotoxicity. On the day of the seeding, an amount of each glue, with and without CATA (1 mg mL^{-1}), was restored with ultrapure sterile water and immersed in DMEM-LG. The extraction was performed for 24 h, at 37 °C. Afterward, on assay day 0, 0.5 mL per well of extraction media from each bioadhesive were put in contact with the seeded cells for evaluation of cytotoxicity on days 1, 3, and 7.

In Vitro Cell Culture and Cell Viability Assessment: An immortalized mouse fibroblast cell line (L929) was cultured in DMEM-LG, supplemented with 10% FBS and 1% antibiotic/antimycotic in 175 cm^2 adherent tissue culture flasks, at 37 °C, in a 5% CO_2 high-humidity environment until being semiconfluent. At 90% confluence, L929 cells were detached using 1 trypsin–EDTA and seeded in adherent or suspension 24 well-plates. In the case of the suspension 24 well-plates, the cells were cultured on coverslips pre-coated with a collagen solution (500 µg mL^{-1}) before seeding. At each pre-settled time point, the metabolic activity of the treated cells was qualitatively and quantitatively assessed by Live-dead and alamarBlue assays, respectively.

For performing the live-dead assay, in the time point day, cells were incubated in a solution of calcein AM (DMSO, Thermo Fisher Scientific, USA, 0.002% (v/v)) and propidium iodide (Thermo Fisher Scientific, USA, 0.001% (v/v)) in PBS, at 37 °C, for 30 min. After incubation, cells were observed using a fluorescence microscope (Fluorescence Microscope Zeiss, Axio Imager 2, Zeiss, Germany). For quantitative assessment of cells' metabolic activity, an alamarBlue fluorescent assay was also carried out at each pre-settled time point. Cells were incubated with 10% v/v alamarBlue (Thermo Fisher Scientific, USA) solution in a warm culture medium for 4 h, at 37 °C ($n = 3$). Every time, three wells of each condition were analyzed, and the fluorescence readings of each well were performed in triplicate (100 µL). The fluorescence was measured using excitation and emission wavelengths of 540 and 600 nm, respectively (Microplate Reader Synergy HTX, Biotek, USA). The viability of the control was regarded as 100%.

Evaluation Assay of Antibacterial Performance: The antibacterial properties of the TA|PUL-MA adhesives were evaluated through a growth-inhibition assay, as described elsewhere.[90] Briefly, the capacity of the TA-based adhesives to inhibit bacterial growth was tested with two example species of Gram-negative and Gram-positive, namely *E. coli* and *S. aureus* American Type Culture Collection cultures. A 20% (w/w) TA solution, the

same used to prepare the adhesive materials, was used as a positive control. Bacteria colonies isolated from nutrient agar were prepared by inoculating them into 5 mL of LB medium (Merck), followed by incubation for 18–24 h in a shaking water bath, at 180 rpm and 37 °C. Then, the obtained bacteria cellular suspensions (1 mL) were centrifuged at 13 000 × *g* for 10 min, the supernatant was discarded, and the resulting pellet suspension was resuspended in an aqueous saline solution (0.9% (w/v) sodium chloride). The cellular density was determined by UV–vis spectroscopy at 600 nm (UV mini-1240 UV-VIS Spectrophotometer; Shimadzu). After inoculum spreading in Mueller Hinton agar medium (nzytech), this was pierced with a 6 mm punch to produce small holes where an amount of each TA|PUL-MA bioadhesive (20 µL) was inserted to carry out the test. The samples were tested with and without the CATA enzyme. Following inoculum spreading in Mueller Hinton agar medium (nzytech), the samples were incubated for 24 h, at 37 °C.[91] In the next day, to calculate the inhibition zone, the diameters around the sample zones were manually measured ($n = 3$). Statistical analysis was performed using GraphPad with two-way ANOVA, with a significance level set at $p < 0.05$.

Blood Clotting Study: Whole blood was obtained under a cooperation agreement between the CICECO – Aveiro Institute of Materials, University of Aveiro and Hospital da Luz (Aveiro, Portugal) after approval of the Competent Ethics Committee (CEC). The blood was collected from healthy human volunteers, in sodium citrate tubes, and handled under the guidelines approved by the CEC. Informed consent was obtained from all subjects. For carrying out the test, the previous citrated blood was maintained at 37 °C in 500 µL aliquots to which 100 µL of a 0.25 M calcium chloride solution was added to recalcify the blood. This sample was allowed to clot and served as the control. For the test samples, 180 mg of each adhesive, with and without CATA enzyme, and its counterparts (i.e., TA, PUL-MA 6% or PUL-MA 13%) was put in contact with the 500 µL of recalcified blood, which was allowed to clot. The time at which there was no blood flow upon inversion was considered the blood clotting time.

Hemostasis Study: Citrated blood from healthy human volunteers obtained from the above-mentioned cooperation agreement was diluted by the addition of a 0.9% (w/v) NaCl solution (1:9) and taken in 500 µL aliquots. To these, 100 µL of 0.1% (w/v) Triton-X (positive control), 100 µL of 0.9% (w/v) NaCl solution (negative control), or 180 mg of the TA|PUL-MA adhesives and their individual counterparts (TA, PUL-MA 6% or PUL-MA 13%) were added and incubated at 37 °C, for 1 h. Afterward, samples were centrifuged (3500 rpm), for 10 min, to obtain plasma, which was then collected (100 µL), and the absorbance (OD value) at 540 nm of each sample was measured. The hemolysis (%) was calculated using the Equation (3)

$$\text{Hemolysis } (\%) = \frac{\text{ODsample} - \text{ODneg}}{\text{ODpos} - \text{ODneg}} \times 100\% \quad (3)$$

Burst Pressure Test: The Burst pressure test was carried out as per ASTM standard procedure with slight modifications (ASTM F 2392–04). An apparatus was built in the lab to carry out the test consisting of a syringe pump (Harvard Apparatus) where a 30 mL syringe was connected to a rubber tube that forks and connects to both a barometer and a support produced by 3D printing (FlashForge Creator 3) of polylactic acid (PLA), to ensure it was leak proof. The test was carried out with wet porcine skin (30 × 30 × 30 cm^3) that was punched, creating a 3.5 mm hole. The porcine skin was adhered to the PLA surface and, prior to the application of the adhesives, the pressure was increased to ensure that the system was leak-proof and it could withstand pressures of ≈250 mmHg, which was significantly greater than normal arterial blood pressure (120 mmHg). 200 mg of sample (TA|PUL-MA 13%) were applied to the 3.5 mm hole and the test was performed immediately after. Upon gradual increase in pressure, the pressure at which leak from the skin portion was verified was noted as the maximum pressure that the applied adhesives withstand.

Statistical Analysis: Statistical analysis was performed with GraphPad Prism 6 (GraphPad Software, California, USA). All results were expressed as mean ± standard deviation with at least three independent assays. Differences between groups were analyzed by one-way or two-way analysis of variance (ANOVA). Statistical significant differences were considered as follows: * = $p < 0.05$, ** = $p < 0.01$, *** = $p < 0.001$, **** = $p < 0.0001$.

Supporting Information

Supporting Information is available from the Wiley Online Library or from the author.

Acknowledgements

This work was developed within the scope of the project CICECO-Aveiro Institute of Materials UIDB/50011/2020 (DOI 10.54499/UIDB/50011/2020), UIDP/50011/2020 (DOI 10.54499/UIDP/50011/2020) &LA/P/0006/2020 (DOI 10.54499/LA/P/0006/2020), financed by national funds through the FCT/MEC (PIDDAC), and within the scope of the project BLUEGLUE (FA_05_2017_031) financed by Fundo Azul (Call – N.° 5/2017) and Direção-Geral de Política do Mar (DGMP) do Ministério Português do Mar. This work was also funded by the European Union's Horizon Europe research and innovation program under the grant agreement No. 101079482 ("SUPRALIFE"). The NMR spectrometers were part of the National NMR Network (PTNMR) and were partially supported by Infrastructure Project N° 022161 (co-financed by FEDER through COMPETE 2020, POCI and PORL, and FCT through PIDDAC). M.M.A.S, M.B.O., J.B., and J.M.M.R. gratefully acknowledge FCT for the PhD grant 2020.07156.BD – M.M.A.S. and individual researcher contracts CEECINST/00013/2021 – M.B.O., 2020.00758.CEECIND (DOI 10.54499/2020.00758.CEECIND/CP1589/CT0007) – J.B., CEECIND/01363/2018 (DOI 10.54499/CEECIND/01363/2018/CP1559/CT0022) – J.M.M.R. under the Scientific Employment Stimulus, respectively.

Conflict of Interest

The authors declare no conflict of interest.

Data Availability Statement

The data that support the findings of this study are available from the corresponding author upon reasonable request.

Keywords

antibacterial, bioadhesive, coacervate, cytocompatible, supramolecular, tannic acid

Received: December 22, 2023
Revised: February 2, 2024
Published online:

[1] Y. Mizuno, R. Mizuta, M. Hashizume, T. Taguchi, *Biomater. Sci.* **2017**, *5*, 982.
[2] H. Huang, H. Chen, X. Wang, F. Qiu, H. Liu, J. Lu, L. Tong, Y. Yang, X. Wang, H. Wu, *ACS Biomater. Sci. Eng.* **2019**, *5*, 5498.
[3] K. Shanmugapriya, H. W. Kang, *Mater. Sci. Eng. C* **2019**, *105*, 110110.
[4] H. Yuk, C. E. Varela, C. S. Nabzdyk, X. Mao, R. F. Padera, E. T. Roche, X. Zhao, *Nature* **2019**, *575*, 169.
[5] K. Kim, M. Shin, M.-Y. Koh, J. H. Ryu, M. S. Lee, S. Hong, H. Lee, *Adv. Funct. Mater.* **2015**, *25*, 2402.
[6] Z. Ma, G. Bao, J. Li, Z. Ma, G. Bao, J. Li, *Adv. Mater.* **2021**, *33*, 2007663.

[7] T. Fattahi, M. Mohan, G. T. Caldwell, *J. Oral Maxillofac. Surg.* **2004**, *62*, 218.
[8] D. García Cerdá, A. M. Ballester, A. Aliena-Valero, A. Carabén-Redaño, J. M. Lloris, *Surg. Today* **2015**, *45*, 939.
[9] H. Ruprai, A. Shanu, D. Mawad, J. M. Hook, K. Kilian, L. George, R. Wuhrer, J. Houang, S. Myers, A. Lauto, *Acta Biomater.* **2020**, *101*, 314.
[10] Y. Liang, X. Zhao, T. Hu, B. Chen, Z. Yin, P. X. Ma, B. Guo, *Small* **2019**, *15*, 1900046.
[11] T. Hasegawa, *Int. J. Mol. Sci.* **2010**, *11*, 1082.
[12] M.-V. Clement, L. H. Long, J. Ramalingam, B. Halliwell, *J. Neurochem.* **2002**, *81*, 414.
[13] H. Meng, Y. Li, M. Faust, S. Konst, B. P. Lee, *Acta Biomater.* **2015**, *17*, 160.
[14] R. Pinnaratip, P. K. Forooshani, M. Li, Y. H. Hu, R. M. Rajachar, B. P. Lee, *ACS Biomater. Sci. Eng.* **2020**, *6*, 4502.
[15] J. Guo, W. Sun, J. P. Kim, X. Lu, Q. Li, M. Lin, O. Mrowczynski, E. B. Rizk, J. Cheng, G. Qian, J. Yang, *Acta Biomater.* **2018**, *72*, 35.
[16] X. Lu, S. Shi, H. Li, E. Gerhard, Z. Lu, X. Tan, W. Li, K. M. Rahn, D. Xie, G. Xu, F. Zou, X. Bai, J. Guo, J. Yang, *Biomaterials* **2020**, *232*, 119719.
[17] X. Peng, Y. Li, T. Li, Y. Li, Y. Deng, X. Xie, Y. Wang, G. Li, L. Bian, *Adv. Sci.* **2022**, *9*, 2203890.
[18] H. Montazerian, S. Mitra, A. Hassani Najafabadi, R. Seyedmahmoud, Y. Zheng, M. R. Dokmeci, N. Annabi, A. Khademhosseini, P. S. Weiss, *ACS Mater. Lett.* **2023**, *5*, 1672.
[19] G. Mugnaini, C. Resta, G. Poggi, M. Bonini, *J. Colloid Interface Sci.* **2021**, *592*, 430.
[20] C. N. Elangwe, S. N. Morozkina, R. O. Olekhnovich, V. O. Polyakova, A. Krasichkov, P. K. Yablonskiy, M. V. Uspenskaya, *Int. J. Mol. Sci.* **2023**, *24*, 4962.
[21] F. Sun, Y. Bu, Y. Chen, F. Yang, J. Yu, D. Wu, *ACS Appl. Mater. Interfaces* **2020**, *12*, 9132.
[22] S. H. Kim, K. Kim, B. S. Kim, Y. H. An, U. J. Lee, S. H. Lee, S. L. Kim, B. G. Kim, N. S. Hwang, *Biomaterials* **2020**, *242*, 119905.
[23] E. Astoricchio, C. Alfano, L. Rajendran, P. A. Temussi, A. Pastore, *Trends Biochem. Sci.* **2020**, *45*, 706.
[24] S. Kim, J. Huang, Y. Lee, S. Dutta, H. Young Yoo, Y. Mee Jung, Y. Jho, H. Zeng, D. S. Hwang, *Proc. Natl. Acad. Sci. USA* **2016**, *113*, E847.
[25] D. Lee, H. Hwang, J. S. Kim, J. Park, D. Youn, D. Kim, J. Hahn, M. Seo, H. Lee, *ACS Appl. Mater. Interfaces* **2020**, *12*, 20933.
[26] M.-B. Coltelli, S. Danti, K. De Clerck, A. Lazzeri, P. Morganti, *J. Funct. Biomater.* **2020**, *11*, 20.
[27] H. Lee, N. F. Scherer, P. B. Messersmith, *Proc. Natl. Acad. Sci. USA* **2006**, *103*, 12999.
[28] A. H. Hofman, I. A. van Hees, J. Yang, M. Kamperman, *Adv. Mater.* **2018**, *30*, 1704640.
[29] Y. Xu, Q. Liu, A. Narayanan, D. Jain, A. Dhinojwala, A. Joy, *Adv. Mater. Interfaces* **2017**, *4*, 1700506.
[30] R. Mizuta, T. Taguchi, R. Mizuta, T. Taguchi, *Macromol. Biosci.* **2017**, *17*, 1600349.
[31] L. Xie, X. Cui, L. Gong, J. Chen, H. Zeng, *Langmuir* **2020**, *36*, 2985.
[32] G. Huang, Z. Tang, S. Peng, P. Zhang, T. Sun, W. Wei, L. Zeng, H. Guo, H. Guo, G. Meng, *Macromolecules* **2022**, *55*, 156.
[33] S. Tabandeh, L. Leon, *Molecules* **2019**, *24*, 868.
[34] M. N. Sundaram, V. Krishnamoorthi Kaliannagounder, V. Selvaprithiviraj, M. Suresh, R. Biswas, A. K. Vasudevan, P. K. Varma, R. Jayakumar, *ACS Sustainable Chem. Eng.* **2018**, *6*, 7826.
[35] J. H. Cho, J. S. Lee, J. Shin, E. J. Jeon, S. An, Y. S. Choi, S.-W. Cho, J. H. Cho, J. S. Lee, J. Shin, E. J. Jeon, S. An, Y. S. Choi, S.-W. Cho, W. S. Cho, *Adv. Funct. Mater.* **2018**, *28*, 1705244.
[36] J. Rönnols, O. Engström, U. Schnupf, E. Säwén, J. W. Brady, G. Widmalm, *ChemBioChem* **2019**, *20*, 2519.
[37] A. M. S. Costa, J. F. Mano, *Chem. Commun.* **2015**, *51*, 15673.
[38] M. Rodahl, F. Höök, B. Kasemo, *Anal. Chem.* **1996**, *68*, 2219.
[39] C. F. V. Sousa, C. A. Saraiva, T. R. Correia, T. Pesqueira, S. G. Patrício, M. I. Rial-Hermida, J. Borges, J. F. Mano, *Biomolecules* **2021**, *11*, 863.
[40] M. Matsusaki, H. Ajiro, T. Kida, T. Serizawa, M. Akashi, *Adv. Mater.* **2012**, *24*, 454.
[41] V. Kozlovskaya, S. Harbaugh, I. Drachuk, O. Shchepelina, N. Kelley-Loughnane, M. Stone, V. V. Tsukruk, *Soft Matter* **2011**, *7*, 2364.
[42] S. A. Bencherif, R. W. Sands, D. Bhatta, P. Arany, C. S. Verbeke, D. A. Edwards, D. J. Mooney, *Proc. Natl. Acad. Sci. USA* **2012**, *109*, 19590.
[43] H. Chen, J. Cheng, L. Ran, K. Yu, B. Lu, G. Lan, F. Dai, F. Lu, *Carbohydr. Polym.* **2018**, *201*, 522.
[44] H. V. Vinters, K. A. Galil, M. J. Lundie, J. C. E. Kaufmann, *Neuroradiology* **1985**, *27*, 279.
[45] B. R. Freedman, O. Uzun, N. M. M. Luna, A. Rock, C. Clifford, E. Stoler, G. Östlund-Sholars, C. Johnson, D. J. Mooney, *Adv. Mater.* **2021**, *33*, 2008553.
[46] A. D. Augst, H. J. Kong, D. J. Mooney, *Macromol. Biosci.* **2006**, *6*, 623.
[47] W. Li, X. Liu, Z. Deng, Y. Chen, Q. Yu, W. Tang, T. L. Sun, Y. S. Zhang, K. Yue, *Adv. Mater.* **2019**, *31*, 1904732.
[48] M. D. Hager, P. Greil, C. Leyens, S. van der Zwaag, U. S. Schubert, *Adv. Mater.* **2010**, *22*, 5424.
[49] D. Yang, Y. Wang, Z. Li, Y. Xu, F. Cheng, P. Li, H. Li, *J. Mater. Chem. C* **2018**, *6*, 1153.
[50] H. G. Nam, M. G. Nam, P. J. Yoo, J. H. Kim, *Soft Matter* **2019**, *15*, 785.
[51] Z. Wang, S. Zhang, S. Zhao, H. Kang, Z. Wang, C. Xia, Y. Yu, J. Li, *Chem. Eng. J.* **2021**, *404*, 127069.
[52] H. Yuk, J. Wu, T. L. Sarrafian, X. Mao, C. E. Varela, E. T. Roche, L. G. Griffiths, C. S. Nabzdyk, X. Zhao, *Nat. Biomed. Eng.* **2021**, *5*, 1131.
[53] J. Li, A. D. Celiz, J. Yang, Q. Yang, I. Wamala, W. Whyte, B. R. Seo, N. V. Vasilyev, J. J. Vlassak, Z. Suo, D. J. Mooney, *Science* **2017**, *357*, 378.
[54] Y. Huang, C. Fan, Y. Liu, L. Yang, W. Hu, S. Liu, T. Wang, Z. Shu, B. Li, M. Xing, S. Yang, *Adv. Healthcare Mater.* **2022**, *11*, 2200939.
[55] S. Razaviamri, K. Wang, B. Liu, B. P. Lee, *Molecules* **2021**, *26*, 559.
[56] H. Xi, Y. Zhang, Y. Xu, W. Y. Yang, X. Jiang, X. Sha, X. Cheng, J. Wang, X. Qin, J. Yu, Y. Ji, X. Yang, H. Wang, *Circ. Res.* **2016**, *118*, 1525.
[57] J. Zhang, B. Gao, B. Ye, Z. Sun, Z. Qian, L. Yu, Y. Bi, L. Ma, Y. Ding, Y. Du, W. Wang, Z. Mao, *Adv. Mater.* **2023**, *35*, 2208571.
[58] C. Ghobril, M. W. Grinstaff, *Chem. Soc. Rev.* **2015**, *44*, 1820.
[59] C. M. Murphy, *Clin. Microbiol. Rev.* **1999**, *12*, 564.
[60] R. Verma, S. K. Verma, K. P. Rakesh, Y. R. Girish, M. Ashrafizadeh, K. S. Sharath Kumar, K. S. Rangappa, *Eur. J. Med. Chem.* **2021**, *212*, 113134.
[61] L. S. F. Leite, C. Pham, S. Bilatto, H. M. C. Azeredo, E. D. Cranston, F. K. Moreira, L. H. C. Mattoso, J. Bras, *ACS Sustainable Chem. Eng.* **2021**, *9*, 8539.
[62] I. Perelshtein, E. Ruderman, A. Francesko, M. M. Fernandes, T. Tzanov, A. Gedanken, *Ultrason. Sonochem.* **2014**, *21*, 1916.
[63] N. Schweigert, A. J. B. Zehnder, R. I. L. Eggen, *Environ. Microbiol.* **2001**, *3*, 81.
[64] K. B. Myint, L. C. Sing, Z. Wei, *APCBEE Proc.* **2013**, *7*, 175.
[65] E. W. Davie, O. D. Ratnoff, *Science* **1964**, *145*, 1310.
[66] J. Margolis, *Nature* **1956**, *178*, 805.
[67] S. Ramström, *Blood Coagulation Fibrinolysis* **2005**, *16*, 447.
[68] J. Chen, W. Cheng, S. Chen, W. Xu, J. Lin, H. Liu, Q. Chen, *Nanoscale* **2018**, *10*, 22818.
[69] S. Guo, M. Yao, D. Zhang, Y. He, R. Chang, Y. Ren, F. Guan, *Adv. Healthcare Mater.* **2022**, *11*, 2101808.
[70] C. Liu, W. Yao, M. Tian, J. Wei, Q. Song, W. Qiao, *Biomaterials* **2018**, *179*, 83.
[71] W. Zheng, Z. Zhang, Y. Li, L. Wang, F. Fu, H. Diao, X. Liu, *Chem. Eng. J.* **2022**, *447*, 137482.
[72] J. Autian, in *Polymers in Medicine and Surgery*, Springer, New York **1975**, pp. 181–203.

[73] American Society for Testing and Materials (ASTM), ASTM E2524-22: Standard Test Method for Analysis of Hemolytic Properties of Nanoparticles, West Conshohocken, PA, USA **2013**.
[74] T. Goyal, C. L. Schmotzer, *Am. J. Clin. Pathol.* **2015**, *143*, 579.
[75] S. P. Mandell, N. S. Gibran, *Expert Opin. Biol. Ther.* **2014**, *14*, 821.
[76] G. M. Taboada, K. Yang, M. J. N. Pereira, S. S. Liu, Y. Hu, J. M. Karp, N. Artzi, Y. Lee, *Nat. Rev. Mater.* **2020**, *5*, 310.
[77] A. Adji, M. F. O'Rourke, *Intern. Med. J.* **2021**, *51*, 13.
[78] N. Ghosh, A. Das, S. Chaffee, S. Roy, C. K. Sen, *Immunity and Inflammation in Health and Disease*, Academic Press, San Diego, CA **2018**, pp. 45–55.
[79] J. S. Lee, J. H. Cho, S. An, J. Shin, S. Choi, E. J. Jeon, S.-W. Cho, *Chem. Mater.* **2019**, *31*, 9614.
[80] C. A. Custódio, R. L. Reis, J. F. Mano, *Biomacromolecules* **2016**, *17*, 1602.
[81] G. Della Giustina, A. Gandin, L. Brigo, T. Panciera, S. Giulitti, P. Sgarbossa, D. D'Alessandro, L. Trombi, S. Danti, G. Brusatin, *Mater. Des.* **2019**, *165*, 107566.
[82] H. J. C. Berendsen, D. van der Spoel, R. van Drunen, *Comput. Phys. Commun.* **1995**, *91*, 43.
[83] M. J. Abraham, T. Murtola, R. Schulz, S. Páll, J. C. Smith, B. Hess, E. Lindahl, *SoftwareX* **2015**, *1–2*, 19.
[84] T. Darden, D. York, L. Pedersen, *J. Chem. Phys.* **1993**, *98*, 10089.
[85] J. Wang, R. M. Wolf, J. W. Caldwell, P. A. Kollman, D. A. Case, *J. Comput. Chem.* **2004**, *25*, 1157.
[86] A. W. Sousa da Silva, W. F. Vranken, *BMC Res. Notes* **2012**, *5*, 367.
[87] H. J. C. Berendsen, J. R. Grigera, T. P. Straatsma, *J. Phys. Chem.* **1987**, *91*, 6269.
[88] R. Kumari, R. Kumar, A. Lynn, *J. Chem. Inf. Model.* **2014**, *54*, 1951.
[89] N. A. Baker, D. Sept, S. Joseph, M. J. Holst, J. A. McCammon, *Proc. Natl. Acad. Sci. USA* **2001**, *98*, 10037.
[90] L. F. Santos, A. Sofia Silva, C. R. Correia, J. F. Mano, *Proc. Natl. Acad. Sci. USA* **2019**, *116*, 5405.
[91] P. I. Siafaka, A. P. Zisi, M. K. Exindari, I. D. Karantas, D. N. Bikiaris, *Carbohydr. Polym.* **2016**, *143*, 90.